AFWAL-TR-88-3085

TWO-DIMENSIONAL NAVIER-STOKES SOLUTION OF THE FLOW OVER A THICK SUPERCRITICAL AIRFOIL WITH STRONG SHOCK-INDUCED SEPARATION

Don W. Kinsey

Aerodynamics and Airframe Branch
Aeromechanics Division

November 1988

Interim Report for Period January 1987 - January 1988

FLIGHT DYNAMICS LABORATORY
AIR FORCE WRIGHT AERONAUTICAL LABORATORIES
AIR FORCE SYSTEMS COMMAND
WRIGHT-PATTERSON AIR FORCE BASE, OHIO 45433-6553

UNCLASSIFIED

SECURITY CLASSIFICATION OF THIS PAGE

ADA203331

REPORT DOCUMENTATION PAGE

Form Approved OMB No. 0704-0188

1a. REPORT SECURITY CLASSIFICATION Unclassified	1b. RESTRICTIVE MARKINGS N/A
2a. SECURITY CLASSIFICATION AUTHORITY N/A	3. DISTRIBUTION/AVAILABILITY OF REPORT Approved for public release; distribution unlimited.
2b. DECLASSIFICATION/DOWNGRADING SCHEDULE N/A	
4. PERFORMING ORGANIZATION REPORT NUMBER(S) AFWAL-TR-88-3085	5. MONITORING ORGANIZATION REPORT NUMBER(S) N/A
6a. NAME OF PERFORMING ORGANIZATION AFWAL 6b. OFFICE SYMBOL (If applicable) FDMM	7a. NAME OF MONITORING ORGANIZATION N/A
6c. ADDRESS (City, State, and ZIP Code) Wright-Patterson AFB OH 45433-6553	7b. ADDRESS (City, State, and ZIP Code) N/A
8a. NAME OF FUNDING/SPONSORING ORGANIZATION AFWAL 8b. OFFICE SYMBOL (If applicable) FDMM	9. PROCUREMENT INSTRUMENT IDENTIFICATION NUMBER N/A
8c. ADDRESS (City, State, and ZIP Code) Wright-Patterson AFB OH 45433-6553	10. SOURCE OF FUNDING NUMBERS PROGRAM ELEMENT NO. 62201F; PROJECT NO. 2404; TASK NO 10; WORK UNIT ACCESSION NO. A1

11. TITLE (Include Security Classification)
Two-Dimensional Navier-Stokes Solution of the Flow Over a Thick Supercritical Airfoil with Strong Shock-Induced Separation

12. PERSONAL AUTHOR(S)
Don W. Kinsey

13a. TYPE OF REPORT	13b. TIME COVERED	14. DATE OF REPORT (Year, Month, Day)	15. PAGE COUNT
Interim	FROM Jan 87 TO Jan 88	Nov 88	74

16. SUPPLEMENTARY NOTATION
N/A

17. COSATI CODES		
FIELD	GROUP	SUB-GROUP
01	01	
01	02	

18. SUBJECT TERMS (Continue on reverse if necessary and identify by block number)
Transonic Aerodynamics; Navier-Stokes, Two-Dimensional, Computational Aerodynamics, Separated Flow.

19. ABSTRACT (Continue on reverse if necessary and identify by block number)

This report describes a numerical solution of the Navier-Stokes equations for transonic flow over a thick supercritical airfoil with strong shock-induced separation on both the upper and lower surfaces. The separated flow region extends from the shock (approximately 50% chord) to the trailing edge on both surfaces.

The first part of this report is basically a review of the processes involved in producing a computational solution of the Navier-Stokes equations for a two-dimensional airfoil in a perfect gas. A brief development of the Navier-Stokes equations is provided. The solution algorithm used (an explicit predictor-corrector method) is developed and described. An algebraic turbulence model used to model the turbulent Reynolds stresses is described and the need for such a model is discussed. A hyperbolic, two-dimensional procedure for producing a computational grid (mesh) is also described. The boundary conditions imposed at the outer regions of the computational (see reverse)

20. DISTRIBUTION/AVAILABILITY OF ABSTRACT	21. ABSTRACT SECURITY CLASSIFICATION
☒ UNCLASSIFIED/UNLIMITED ☐ SAME AS RPT. ☐ DTIC USERS	Unclassified

22a. NAME OF RESPONSIBLE INDIVIDUAL	22b. TELEPHONE (Include Area Code)	22c. OFFICE SYMBOL
Don W. Kinsey	513-255-2481	AFWAL/FDMM

DD Form 1473, JUN 86 Previous editions are obsolete. SECURITY CLASSIFICATION OF THIS PAGE

UNCLASSIFIED

A

Block 19 Continued:

domain (farfield) and at the airfoil surface are discussed and described.

The second part of the report discusses the treatment of the eddy viscosity development through the shock, in the separated regions over the airfoil and in the near wake. This work was critical for obtaining a successful solution on the very difficult test case chosen. Modifications to an algebraic eddy viscosity model to include the effects of the thickness of the separated flow region downstream of the shock are described.

FOREWORD

This report was prepared by Don W. Kinsey of the Aerodynamics and Airframe Branch, Aeromechanics Division, Flight Dynamics Laboratory, Wright-Patterson AFB, Ohio. This work was performed under Work Unit 240410A1 during the period of January 1987 to January 1988.

This attempt to extend the useful range of the two-dimensional Navier-Stokes solver to include flow with strong shock-induced separation is part of a continuing effort to study transonic aerodynamics.

TABLE OF CONTENTS

LIST OF ILLUSTRATIONS

LIST OF ILLUSTRATIONS

LIST OF TABLES

I. INTRODUCTION

Background

Progress in obtaining general solutions to viscous fluid flow problems has been very slow and difficult. It was over 230 years ago that Euler (1755) derived the equations for frictionless fluid flow.[1] It was another 70 years before Navier (1827) added viscous terms to Euler's equations. Soon after that Stokes (1845) improved Navier's idea by the introduction of the coefficient of viscosity, μ, that defined the fluid stress as proportional to the rate-of-change of strain. Thus, the equations governing the flow of a viscous fluid (Navier-Stokes equations) have been known for over 140 years. However, only a few special-case solutions to these equations have been found analytically. The equations are simply too difficult to solve analytically for general flow problems. Fortunately the recent development of large, efficient computers has opened the way for numerical solutions of the governing equations.

This section will show how the steady, two-dimensional Navier-Stokes equations are formulated for numerical solutions and how this solution is obtained. Much of this information is available from text books and other sources but it is summarized here for convenience and completeness. Also included is a discussion of the necessity for, and the application of, a turbulence model for estimating the effects of a turbulent boundary layer.

The remainder of the report describes the modifications made to the turbulence model in order to get a successful solution, and a discussion of the results for transonic flow over a thick supercritical airfoil. The thick supercritical airfoil was chosen for this study because it provided the most severe flow conditions the author could find for which experimental data were available.

Governing Equations

The Navier-Stokes equations can be derived by applying the principles of conservation of mass, conservation of momentum, and conservation of energy to a control volume[2]. Using an Eulerian formulation and assuming an arbitrary control volume V with surface area A, we can express the conservation of mass as:

Rate of mass loss in the control volume
equals net flow of mass out through
the surface.

$$-\frac{\partial}{\partial t}\iiint \rho \, dV = \iint \rho \, \vec{U} \cdot d\vec{A} \qquad (1)$$

Where,

t = time

ρ = density (mass per unit volume)

$\vec{U}$ = total velocity vector.

Similarly, the conservation of momentum (or Newton's second law) states:

The sum of the external forces equals the
rate of change of momentum.

$$\iint \vec{\vec{P}} \cdot d\vec{A} = \iiint \rho \, \frac{D\vec{U}}{Dt} \, dV \qquad (2)$$

Where,

$\vec{\vec{P}}$ = a dyadic representing the normal and shear stresses acting on the control volume. All other forms of external forces are assumed to be negligible.

$\frac{D\vec{U}}{Dt}$ = the substantial derivative which represents the sum of the local change in the variable plus the convective rate-of-change.

$$\frac{D\vec{U}}{Dt} \equiv \frac{\partial \vec{U}}{\partial t} + \vec{U} \cdot \nabla\vec{U}$$

Finally, the conservation of energy states:

The rate-of-change of energy in the control

volume equals the rate of heat added through the surface plus the rate of work done by external forces.

$$\iiint \rho \frac{De}{Dt} dV = \iint \dot{q}.d\vec{A} + \iint (\vec{\vec{P}}.\vec{U}).d\vec{A} \qquad (3)$$

Where,

e = internal energy per unit mass (specific internal energy plus kinetic energy, all other energy terms are assumed to be negligible)

$\dot{q}$ = heat flux vector.

This formulation assumes there is no energy source or sink within the control volume.

Notice that equation (2) is a vector equation and represents the conservation of momentum in each dimension of interest (x and y for a two-dimensional problem in Cartesian coordinates). Also at the beginning of this section it was stated that the control volume was of arbitrary size; however, it is assumed to contain enough molecules to represent a continuum[3].

It is possible to develop a numerical solution procedure to solve the governing equations in integral form. For example, Jameson[4] uses Runge-Kutta integration techniques over finite-volumes to solve the Euler equations (equations 1-3 without the viscous stresses). However, the numerical method used in the present study requires a differential form of the equations. This is accomplished by applying Gauss' divergence theorem to the integral equation and making an argument about the arbitrary size of the control volume V. Gauss' divergence theorem equates surface integrals to volume integrals and is written as:

$$\iint \vec{\vec{Q}} \cdot d\vec{A} = \iiint (\nabla \cdot \vec{\vec{Q}}) \, dV. \qquad (4)$$

Where,

$\vec{\vec{Q}}$ = any tensor quantity that is first-order continuous,

∇ = the divergence operator.

Applying Gauss' divergence theorem to the right-hand side of equation (1) yields;

$$\iiint (\nabla . \rho\vec{U})\ dV + \frac{\partial}{\partial t} \iiint \rho\ dV = 0. \tag{5}$$

If the control volume is not a function of time, the order of integration and differentiation may be reversed and equation (5) may be written as:

$$\iiint \left[(\nabla . \rho\vec{U}) + \frac{\partial \rho}{\partial t}\right] dV = 0. \tag{6}$$

At this point the argument is made that if the control volume is arbitrary, the integrand itself must vanish if the integral is to be zero. Therefore,

$$\frac{\partial \rho}{\partial t} + \nabla\ .\ \rho\vec{U} = 0 \tag{7}$$

is the derivative form of the conservation of mass. Following a similar procedure equation (2) may be written as;

$$\rho \frac{D\vec{U}}{Dt} - \nabla\ .\ \vec{\vec{P}} = 0 \tag{8}$$

and equation (3) may be written as;

$$\rho \frac{De}{Dt} - \nabla.(\vec{\vec{P}}.\vec{U} + \vec{q}) = 0 \tag{9}$$

Equations (8) and (9) still contain substantial derivative terms. These may be written in a more convenient form by using the definition of the substantial derivative and making use of the conservation of mass equation. The equations then become:

Continuity

$$\frac{\partial \rho}{\partial t} + \nabla.\rho\vec{U} = 0 \tag{10}$$

Momentum

$$\frac{\partial \rho\vec{U}}{\partial t} + \nabla.(\rho\vec{U}\vec{U} - \vec{\vec{P}}) = 0 \tag{11}$$

Energy

$$\frac{\partial \rho e}{\partial t} + \nabla.(\rho\vec{U}e - \vec{\vec{P}}.\vec{U} - \vec{q}) = 0. \tag{12}$$

Equations (10), (11) and (12) are the classic Navier-Stokes equations for compressible fluid flow without body forces or energy loss or gain within the domain of interest. However, the system of equations is not closed and several variables need clarification before practical solutions can be obtained.

The heat flux ($\vec{q}$) is determined from Fourier's law as;

$$\vec{q} = \hat{k} \nabla T$$

Where

T = the temperature

$\hat{k}$ = the thermal conductivity.

The value of $\hat{k}$ for fluids is a thermodynamic property that varies as a function of temperature.

The most complicated variable in the Navier-Stokes equations is the stress tensor ($\vec{\vec{P}}$). In a two-dimensional Cartesian coordinate system $\vec{\vec{P}}$ can be written as

$$\vec{\vec{P}} = \begin{bmatrix} \tau_{xx} & \tau_{xy} \\ \tau_{yx} & \tau_{yy} \end{bmatrix} \tag{13}$$

where,

τ_{xx} = the normal stress in the x direction

τ_{yy} = the normal stress in the y direction

τ_{xy} = the shear stress on the x face in the y direction

τ_{yx} = the shear stress on the y face in the x direction.

It is at this point that Stokes' work becomes very important. He postulated that the stress is a linear function of strain rates, that a fluid is isotropic, and that the normal stress must equal the hydrostatic pressure when the fluid is at rest. Using these assumptions and defining two additional variables μ and λ, assumed to be properties of the fluid, the stresses may be defined as

$$\tau_{xx} = -p + 2\mu\frac{\partial u}{\partial x} + \lambda\left(\frac{\partial u}{\partial x} + \frac{\partial v}{\partial y}\right)$$

$$\tau_{yy} = -p + 2\mu\frac{\partial v}{\partial y} + \lambda\left(\frac{\partial u}{\partial x} + \frac{\partial v}{\partial y}\right)$$

$$\tau_{xy} = \mu\left(\frac{\partial u}{\partial y} + \frac{\partial v}{\partial x}\right)$$

$$\tau_{yx} = \mu\left(\frac{\partial v}{\partial x} + \frac{\partial u}{\partial y}\right)$$

where p is the hydrostatic pressure. μ is the coefficient of shear viscosity and is a thermodynamic property of the fluid, usually computed from Sutherland's formula[1]. λ is much more controversial. Fortunately the value for λ has little effect on the solutions of interest in this report. The most commonly accepted method of determining the value of λ for air is to again follow Stokes' lead and set $\lambda = -(2/3)\,\mu$. This forces the trace of $\vec{\vec{P}}$ to be the hydrostatic pressure, p.

The velocity vector $\vec{U}$ for two-dimensional Cartesian coordinates may be defined in terms of u, the component in the x direction and v, the component in the y direction. Thus equation (11) may be separated into two scalar equations. This leaves a system of four equations with six unknowns (u, v, p, T, e, ρ). Obviously some other relationships are required. The additional relationships may be determined by assuming the fluid of interest (air) obeys the perfect gas law. This provides a relationship between density, pressure and temperature,

$$p = \rho RT \tag{15}$$

where R is the gas constant, a known quantity for a given gas. The perfect gas assumption also provides a relationship between internal energy and temperature,

$$e_i = C_v T$$

where,

e_i = the specific internal energy per unit mass

C_v = the constant volume specific heat.

While in reality C_v is a function of temperature, it is essentially constant for practical transonic applications. The total internal energy is the sum of the specific internal energy and the kinetic energy.

$$e = C_v T + 1/2\,(u^2 + v^2) \tag{16}$$

This provides a system of six equations and six unknowns. Notice that equations (15) and (16) may be used to compute pressure and temperature in terms of the other flow variables. Thus a system of four equations in four unknowns (u, v, ρ, e) may be established. These four equations are repeated here as they would be written for a two-dimensional Cartesian coordinate system.

Continuity

$$\frac{\partial \rho}{\partial t} + \frac{\partial \rho u}{\partial x} + \frac{\partial \rho v}{\partial y} = 0 \tag{17a}$$

Momentum

$$\frac{\partial \rho u}{\partial t} + \frac{\partial}{\partial x}(\rho u^2 - \tau_{xx}) + \frac{\partial}{\partial y}(\rho vu - \tau_{yx}) = 0 \tag{17b}$$

$$\frac{\partial \rho v}{\partial t} + \frac{\partial}{\partial x}(\rho uv - \tau_{xy}) + \frac{\partial}{\partial y}(\rho v^2 - \tau_{yy}) = 0 \tag{17c}$$

Energy

$$\frac{\partial \rho e}{\partial t} + \frac{\partial}{\partial x}(\rho ue - u\tau_{xx} - v\tau_{yx} - k\frac{\partial T}{\partial x}) +$$

$$\frac{\partial}{\partial y}(\rho ve - v\tau_{yy} - u\tau_{xy} - k\frac{\partial T}{\partial y}) = 0 \tag{17d}$$

It is convenient to define the primary flow variables as ρ, ρu, ρv, and ρe. Temperature and pressure are inherent in the equations, but can be computed from the four primary variables using equations (15) and (16).

It is also convenient to express equations (17) in flux vector form.

$$\frac{\partial U}{\partial t} + \frac{\partial F}{\partial x} + \frac{\partial G}{\partial y} = 0 \tag{18}$$

Where U here is not the velocity vector but is the vector of the dependent variables. This traditional convention is retained even at the risk of some confusion. F and G are flux vectors.

$$U = \begin{bmatrix} \rho \\ \rho u \\ \rho v \\ \rho e \end{bmatrix}$$

$$F = \begin{bmatrix} \rho u \\ \rho uu - \tau_{xx} \\ \rho uv - \tau_{xy} \\ \rho ue - u\tau_{xx} - v\tau_{yx} - k\frac{\partial T}{\partial y} \end{bmatrix}$$

$$G = \begin{bmatrix} \rho v \\ \rho vu - \tau_{yx} \\ \rho vv - \tau_{yy} \\ \rho ve - v\tau_{yy} - u\tau_{xy} - k\frac{\partial T}{\partial y} \end{bmatrix}$$

$\tau_{xy} = \tau_{yx}$ is assumed for the stress terms.

Generalized Transformation

Flow solutions may be computed by numerically solving equation (18) on an appropriate Cartesian computational grid. In general, however, the body about which the flow solution is desired does not coincide with the grid lines of a Cartesian grid. As a result, it is very difficult to obtain adequate grid resolution near the solid body surface, and the boundary conditions at the surface are difficult to enforce accurately. Therefore, a body conforming computational grid is usually established and the necessary transformations from the Cartesian to the computational coordinate system are performed. The resulting equation is

similar to equation (18), but tedious mathematics are required to obtain a generalized transformation. Use of matrix representation and the notation $\frac{\partial Q}{\partial x} = Q_x$ will be used to help simplify the following development.

The grid points in the body conforming grid are usually defined in terms of locations in a Cartesian coordinate system. That is, if ξ and η represent the transformed coordinate system, the computational grid is defined as;

$$\xi = \xi(x,y)$$
$$\eta = \eta(x,y)$$

The total differentials for ξ and η are defined by;

$$d\xi = \xi_x\, dx + \xi_y\, dy$$
$$d\eta = \eta_x\, dx + \eta_y\, dy$$

Or in matrix form;

$$\begin{bmatrix} d\xi \\ d\eta \end{bmatrix} = \begin{bmatrix} \xi_x & \xi_y \\ \eta_x & \eta_y \end{bmatrix} \begin{bmatrix} dx \\ dy \end{bmatrix} \tag{19}$$

The reverse transformation is:

$$x = x(\xi,\eta)$$
$$y = y(\xi,\eta)$$

and the matrix looks like:

$$\begin{bmatrix} dx \\ dy \end{bmatrix} = \begin{bmatrix} x_\xi & x_\eta \\ y_\xi & y_\eta \end{bmatrix} \begin{bmatrix} d\xi \\ d\eta \end{bmatrix} \tag{20}$$

Multiplying (20) by the inverse of the partial derivative matrix and comparing the results with (19) provides:

$$\begin{bmatrix} d\xi \\ d\eta \end{bmatrix} = \begin{bmatrix} \xi_x & \xi_y \\ \eta_x & \eta_y \end{bmatrix} \begin{bmatrix} dx \\ dy \end{bmatrix} = \begin{bmatrix} x_\xi & x_\eta \\ y_\xi & y_\eta \end{bmatrix}^{-1} \begin{bmatrix} dx \\ dy \end{bmatrix}$$

That is, the matrix of the partial derivatives of the body conforming grid is equal to the inverse of the matrix of partial derivatives of the Cartesian coordinates. Linear algebra techniques provide:

$$\begin{bmatrix} \xi_x & \xi_y \\ \eta_x & \eta_y \end{bmatrix} = \begin{bmatrix} x_\xi & x_\eta \\ y_\xi & y_\eta \end{bmatrix}^{-1} = \frac{\begin{bmatrix} y_\eta & -x_\eta \\ -y_\xi & x_\xi \end{bmatrix}}{\begin{vmatrix} x_\xi & x_\eta \\ y_\xi & y_\eta \end{vmatrix}}$$

If the determinant, called the Jacobian (J) of the transformation, is non-zero, a one-to-one mapping exists such that:

$$\begin{aligned} \xi_x &= y_\eta / J \\ \xi_y &= -x_\eta / J \\ \eta_x &= -y_\xi / J \\ \eta_y &= x_\xi / J \end{aligned} \tag{21}$$

A form of the chain rule states that if

$$F = F(\xi, \eta)$$

and

$$\begin{aligned} \xi &= \xi(x,y) \\ \eta &= \eta(x,y) \end{aligned}$$

then

$$F_x = F_\xi \xi_x + F_\eta \eta_x$$

and similarly,

$$G_y = G_\xi \xi_y + G_\eta \eta_y . \tag{22}$$

Substituting equations (22) into the governing equation (18) provides:

$$U_t + \xi_x F_\xi + \eta_x F_\eta + \xi_y G_\xi + \eta_y G_\eta = 0.$$

Using the definitions in equation (21) and multiplying by J provides:

$$J\, U_t + y_\eta F_\xi - x_\eta G_\xi + x_\xi G_\eta - y_\xi F_\eta = 0.$$

Grouping similar derivatives together and adding terms to keep the equation balanced yields:

$$J\,U_t + (y_\eta F - x_\eta G)_\xi + (x_\xi G - y_\xi F)_\eta +$$
$$(-Fy_{\eta\xi} + Gx_{\eta\xi} - Gx_{\xi\eta} + Fy_{\xi\eta}) = 0 \qquad (23)$$

If the functions $x = x(\xi,\eta)$ and $y = y(\xi,\eta)$ are continuous to at least the second derivative, $x_{\eta\xi} = x_{\xi\eta}$ and $y_{\eta\xi} = y_{\xi\eta}$ and the last terms in parenthesis in equation (23) vanish. The finite difference representation (discussed below) of these metrics must also vanish or errors will be introduced into the finite difference solutions[5].

Redefine the variables in equation (23) such that:

$$U' = J\,U$$

$$F' = y_\eta F - x_\eta G$$

$$G' = x_\xi G - y_\xi F$$

and the transformed equation of motion is:

$$\frac{\partial U'}{\partial t} + \frac{\partial F'}{\partial \xi} + \frac{\partial G'}{\partial \eta} = 0 \qquad (24)$$

This is the strong conservation form of the transformed governing equations. Conservation form is defined by Ref. 5 as a form where the derivatives of the dependent variables have only constant coefficients. Strong conservation form means there are no source terms (right hand side = 0). Conservation is very important for correctly computing strong flow discontinuities (shocks).

The same techniques used to solve the equations (18) for a Cartesian grid can now be applied to the body conforming grid. It is important to remember that F' and G' contain derivatives in the viscous and heat transfer terms that must be properly evaluated in the transformed system.

Considerable effort went into defining the governing equations in terms of x_ξ, x_η, y_ξ and y_η rather that ξ_x, η_x, ξ_y and η_y. This was done because typically the numerical approximations,

$$\xi_x = \frac{\Delta\xi}{\Delta x}\Big|_{\Delta y=0}$$

for example, are not easily determined from a body conforming computational grid. Whereas, the approximation,

$$x_\xi = \left.\frac{\Delta x}{\Delta \xi}\right|_{\Delta\eta=0}$$

is easily determined from the known computational grid.

Finite Difference Approximations

Finite difference solution procedures require the substitution of a finite difference approximation in place of the differential expression. The solution proceeds across the region of interest by taking small steps in the spatial direction at small steps in time. The size of the spatial and temporal steps are critical both for accuracy of the solution and stability of the finite difference approximation. More information on both the grid (spatial steps) and stability will be provided later.

To see how the finite difference approximations are determined, consider the definition of the partial derivative for $f(x,y)$ at $x=x_o$, $y=y_o$,

$$\frac{\partial f(x,y)}{\partial x} = \lim_{\Delta x \to 0} \frac{f(x_o+\Delta x, y_o) - f(x_o, y_o)}{\Delta x}$$

Therefore, in the limit as Δx approaches zero the approximation approaches the exact value. A more enlightening method of developing finite difference approximations is derived from using the Taylor-series expansion for $f(x+\Delta x,y)$:

$$f(x+\Delta x,y) = f(x,y) + \frac{\partial f}{\partial x}\Delta x + \frac{\partial^2 f}{\partial x^2}\frac{\Delta x^2}{2!} + \frac{\partial^3 f}{\partial x^3}\frac{\Delta x^3}{3!} + \ldots . \tag{25}$$

Solving for $\partial f/\partial x$ provides:

$$\frac{\partial f}{\partial x} = \frac{f(x+\Delta x,y) - f(x,y)}{\Delta x} - \frac{\partial^2 f}{\partial x^2}\frac{\Delta x}{2!} + \ldots \tag{26}$$

The truncation error associated with approximating the partial derivative by the first term on the right of the equal sign is the sum of the

remaining terms on the right-hand side. This is described as a finite difference approximation to the partial derivative that is of the order of (0) Δx, or "first-order accurate." Equation (26) is also referred to as a "forward" difference. A "backward" difference is obtained by expanding $f(x-\Delta x,y)$ in a Taylor-series such that;

$$f(x-\Delta x,y) = f(x,y) - \frac{\partial f}{\partial x}\Delta x + \frac{\partial^2 f}{\partial x^2}\frac{\Delta x^2}{2!} - \frac{\partial^3 f}{\partial x^3}\frac{\Delta x^3}{3!} + \ldots \tag{27}$$

then

$$\frac{\partial f}{\partial x} = \frac{f(x,y) - f(x-\Delta x,y)}{\Delta x} + \frac{\partial^2 f}{\partial x^2}\frac{\Delta x}{2!} + \ldots \tag{28}$$

which is again $0(\Delta x)$ or first-order accurate. A higher order accurate approximation may be obtained by subtracting equation (27) from equation (25). This provides;

$$f(x+\Delta x,y)-f(x-\Delta x,y) = 2\frac{\partial f}{\partial x}\Delta x + 2\frac{\partial^3 f}{\partial x^3}\frac{\Delta x^3}{3!} + \ldots \tag{29}$$

Solving equation (29) for the partial derivative provides;

$$\frac{\partial f}{\partial x} = \frac{f(x+\Delta x,y) - f(x-\Delta x,y)}{2\,\Delta x} + 0(\Delta x)^2 \ldots \tag{30}$$

Equation (30) is a "central" difference and is "second-order accurate." Note that the central difference approximation does not use the value of the variable at the point (x,y) of interest.

Finite differences for second order (and higher) derivatives can also be determined. If equations (25) and (27) are added together the result is;

$$f(x+\Delta x,y) + f(x-\Delta x,y) = 2f(x,y) + 2\frac{\partial^2 f}{\partial x^2}\frac{(\Delta x)^2}{2!} + 0(\Delta x)^4$$

Solving for the second derivative;

$$\frac{\partial^2 f}{\partial x^2} = \frac{f(x+\Delta x,y) - 2f(x,y) + f(x-\Delta x,y)}{(\Delta x)^2} + 0(\Delta x)^2 \tag{31}$$

Equation (31) is a second-order accurate central difference for the second derivative. These are but a few of the many possible finite difference approximations. A good summary of forward, central and backward differences for first-through fourth-order differences is provided in Ref. 6. Similar finite difference approximations exist for derivatives with respect to y and/or time. Mixed partial derivatives are also possible and a summary table is provided in Ref. 5. The spatial step sizes are determined by the computational grid, and the temporal step size is most often determined by stability considerations.

The archetypal partial differential equation for demonstrating finite difference methods is the one-dimensional linear hyperbolic convection equation;

$$\frac{\partial u}{\partial t} + c\,\frac{\partial u}{\partial x} = 0 \qquad c > 0 \text{ is constant}$$

Substituting a forward difference approximation for time and a central difference for space provides;

$$\frac{u(t+\Delta t,x) - u(t,x)}{\Delta t} + c\,\frac{u(t,x+\Delta x) - u(t,x-\Delta x)}{2\,\Delta x} = 0.$$

Solving for $u(t+\Delta t,x)$;

$$u(t+\Delta t,x) = (c/2)\left(\frac{\Delta t}{\Delta x}\right)[u(t,x-\Delta x) - u(t,x+\Delta x)] + u(t,x) \qquad (32)$$

Equation (32) is called an explicit method (Euler explicit to be exact) because the value at the next time step is explicitly known in terms of values at the current time step. The solution would be obtained by dividing the domain into small spatial increments (grid), applying the appropriate boundary conditions and iterating in time with small temporal increments. Explicit schemes typically have very restrictive time step requirements in order to avoid small errors from amplifying and destroying the solution. In fact, a von Neumann stability analysis[5,7] indicates that the explicit Euler method is unstable for any time step.

If equation (32) were rewritten with the spatial difference evaluated at the next time step, rather than the current time step, we obtain;

$$u(t+\Delta t,x) = (c/2)\left(\frac{\Delta t}{\Delta x}\right)[u(t+\Delta t,x-\Delta x) -$$

$$u(t+\Delta t, x+\Delta x)] + u(t,x) \qquad (33)$$

Equation (33) is called an Euler implicit method. A stability analysis indicates the method would be stable for any time step; however, a set of simultaneous equations must be solved at each iteration. Implicit schemes typically are very stable and allow relatively large time steps that are limited by truncation errors rather than stability. Unfortunately, very large computational domains require the solution of a large set of simultaneous equations which may take considerable computer time.

It is obvious that the large number of possible finite difference approximations available for a given partial differential equation provides for an almost endless number of possible solution schemes. Many such methods are described in Refs. 5 and 7. New methods and variations of the old methods will undoubtedly continue to evolve for some time to come. Any new or modified solution method must be accompanied by a stability analysis to determine the allowable step size. Unfortunately the mathematics associated with such an analysis is prohibitively difficult for complex partial differential equations. Often an approximate stability criterion is determined from analysis of a simplified version of the governing equation, and then the final stability criterion is determined by trial-and-error.

The solution procedure chosen for this study is the MacCormack explicit method, described in Ref. 8. The advantages associated with this method are that it is relatively simple, is easily vectorized on supercomputers and provides a good solution at flow discontinuities (shocks). The primary disadvantage is that the restriction on the allowable time step requires many iterations for a converged solution.

MacCormack's method is called a two-step or a predictor-corrector procedure. The first step, or predictor, is a first-order forward difference in both time and space. The second step (or corrector) is a first order backward difference in space. The net result is said[8] to be second-order accurate in both time and space. The exact derivation of MacCormack's method is obscure. Hankey[2] provides the following finite

difference "MacCormack" representation for the linear convection equation;

Predictor

$$\frac{\overset{*}{u}(t+\Delta t,x) - u(t,x)}{\Delta t} + c\left(\frac{u(t,x+\Delta x) - u(t,x)}{\Delta x}\right)=0 \qquad (34)$$

Corrector

$$\frac{u(t+\Delta t,x) - u(t,x)}{\Delta t} + c\left(\frac{\overset{*}{u}(t,x) - \overset{*}{u}(t,x-\Delta x)}{\Delta x}\right) +$$

$$(c/2)\left(\frac{u(t,x+\Delta x) - u(t,x)}{\Delta x}\right) = 0. \qquad (35)$$

Where $\overset{*}{u}$ represents an intermediate (predicted) solution. An intermediate value of the flow variable is determined at each point in the grid by solving the predictor equation;

$$\overset{*}{u}(t+\Delta t,x) = u(t,x) - c(\Delta t/\Delta x)[u(t,x+\Delta x)-u(t,x)]. \qquad (36)$$

Solving the corrector equation (35) for $u(t+\Delta t)$ by making use of the definition of $\overset{*}{u}$ from the predictor equation (34) provides;

$$u(t+\Delta t,x)=(1/2)\{u(t,x) + \overset{*}{u}(t,x) -$$

$$(\Delta t/\Delta x)[\overset{*}{u}(t,x) - \overset{*}{u}(t,x-\Delta x)]\}. \qquad (37)$$

Equations (36) and (37) are the accepted predictor and corrector expression for the MacCormack method.

The corrector equation represents a forward-time, backward-space difference. However, it is not clear where the last term in equation (35) comes from. Ref. 5 indicates that MacCormack's scheme is a variation of the two-step Lax-Wendroff procedure, which uses averaging and half-step techniques. Therefore, a possible finite difference interpretation for the corrector step that would also reduce to equation (37) is;

$$\frac{u(t+\Delta t,x) - (1/2)[\overset{*}{u}(t,x) + u(t,x)]}{(1/2)\ \Delta t}$$

$$+ c\left[\frac{\overset{*}{u}(t,x) - \overset{*}{u}(t,x-\Delta x)}{\Delta x}\right] = 0$$

This provides a true backward difference for the spatial derivative (of the predicted variable) but assumes that the average of the original variable and the predicted variable constitutes half of the time step between the old and new iteration.

Recall that the vector form of the Navier-Stokes equations (18) was;

$$\frac{\partial U}{\partial t} + \frac{\partial F}{\partial x} + \frac{\partial G}{\partial y} = 0.$$

In order to simplify the notation the following convention will be followed in the preceding equations:

n represents the current time step,

i represents the current x location,

j represents the current y location,

Δt is the time increment between n and n+1,

Δx is the spatial increment between i and i+1 or i and i-1,

Δy is the spatial increment between j and j+1 or j and j-1.

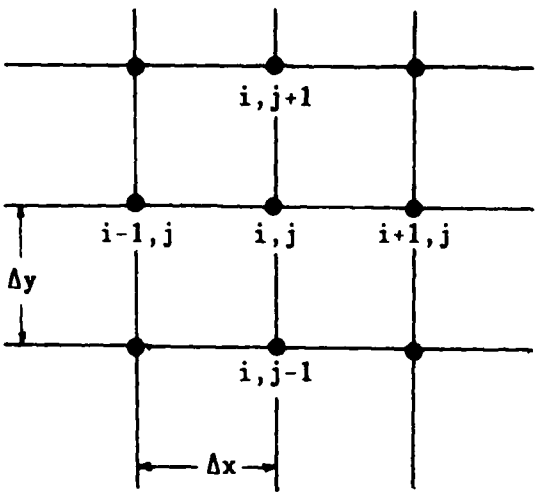

Therefore, the forward time, forward space representation for the governing equation in MacCormack's predictor-corrector form is:

$$\bar{U}^{n+1}_{i,j} = U^{n}_{i,j} - (\Delta t/\Delta x)(F^{n}_{i+1,j} - F^{n}_{i,j}) -$$

$$(\Delta t/\Delta y)(G^{n}_{i,j+1} - G^{n}_{i,j}). \tag{38}$$

Equation (38) is used to determine an intermediate (predictor) value for the flow variables at each point in the computational grid. The corrector step is written:

$$U^{n+1}_{i,j} = (1/2)[U^{n}_{i,j} + \overset{*}{U}^{n+1}_{i,j} - (\Delta t/\Delta x)(\overset{*}{F}^{n+1}_{i,j} - \overset{*}{F}^{n+1}_{i-1,j})$$
$$- (\Delta t/\Delta x)(\overset{*}{G}^{n+1}_{i,j} - \overset{*}{G}^{n+1}_{i,j-1})]$$

where $\overset{*}{F}$ and $\overset{*}{G}$ are computed using the intermediate, or predictor, values of the vector $\overset{*}{U}$.

MacCormack[8] attempted a stability analysis of a two-dimensional linearized version of the governing equations. After some rationalization and much mathematics he arrived at the stability criterion;

$$\Delta t \leq [\Delta x/(|u| + |v| + 2c)]^{4/3} \tag{39}$$

A one-dimensional analysis provided the Courant-Friedrichs-Lewy (CFL)[9] condition;

$$\Delta t \leq [\Delta x/(|u| + c)]. \tag{40}$$

For small spatial grid increments equation (39) is much more restrictive than equation (40). MacCormack ignores viscous and heat transfer effects by stating they will not affect stability providing;

$$(\mu/\rho)(\Delta t/\Delta x^{2}) < 1$$

and

$$k(\Delta t/\Delta x^{2}) < 1.$$

In practice, these criteria may become dominant in the high gradient regions of a boundary layer where very small spatial increments are defined. Ref. 5 suggests an empirical formula for Δt that is based on the CFL and grid mesh Reynolds number.

Strong flow discontinuities (shocks) can produce large gradients across grid cells. The resulting numerical oscillations may be large enough to cause the solution procedure to fail. To help avoid these numerical anomalies most solution procedures provide some method of

numerical smoothing (also called damping or artificial viscosity). The objective is to produce the necessary moderation of the numerical oscillations without affecting the physics of the flow. Usually smoothing corrections of the order of the truncation error or smaller are employed. MacCormack[8] has developed a fourth order smoothing term that is proportional to the second derivative of the pressure. The form of the smoothing is;

$$\hat{\alpha}\ \Delta t\ (\Delta x)^3\ \ \frac{\partial}{\partial x}\left[\frac{|u| + c}{4p}\left|\frac{\partial^2 p}{\partial x^2}\right|\ \frac{\partial \vec{U}}{\partial x}\right]$$

where $\hat{\alpha}$ is a constant such that $0 \leq \hat{\alpha} \leq 0.5$.

For most flow problems this smoothing term will be very small except in the region of large pressure gradients, such as near strong shocks. Some smearing of the shocks over two or more grid cells is inevitable with this approach. Different solution algorithms and/or adaptive grid routines may help minimize the smoothing effects.

Turbulence Models

The Navier-Stokes equations model any fluid flow that meets the assumptions made in their derivation. Unfortunately, turbulent boundary layers present a situation which, while theoretically predictable via the Navier-Stokes equations, is not practical to do so because of the size and the random frequencies of the turbulent structures in a high Reynolds number flow. Numerical resolution of these turbulent structures would require such a fine grid (10^5 points per cubic centimeter[5]) that it is said that the fastest computer would take many years to solve the relatively simple problem of turbulent flow in a pipe[1].

Since direct calculation of the small scale turbulent flow structures was not a viable option, researchers found ways of approximating the mean flow characteristics of turbulent boundary layers. The resulting equations are the time-averaged or Reynolds-averaged Navier-Stokes equations. The solution approach is to solve the Reynolds-averaged equations for the mean flow (large scale flow features) while modeling

the fluctuating effects (small scale flow structures) by some other method.

In the classical Reynolds averaging the primary flow variables are replaced by the sum of a time-averaged term and a fluctuating term. For example, if f is an arbitrary flow variable, then

$$f \equiv \bar{f} + f',$$

where $\bar{f}$ is the steady or time-averaged value;

$$\bar{f} \equiv \frac{1}{\Delta t} \int_{t_o}^{t_o+\Delta t} f \, dt,$$

and f' is the deviation from this mean. Δt is a time increment of sufficient length to provide a statistically significant result. By definition, the time average of the fluctuating part is zero. That is;

$$\bar{f}' \equiv \frac{1}{\Delta t} \int_{t_o}^{t_o+\Delta t} f' \, dt \equiv 0.$$

However, the time-average of the products of the fluctuating properties is <u>not</u> zero ($\overline{f' f'} > 0$).

To demonstrate the Reynolds averaging process, the continuity equation (10) for one dimension is written as;

$$\frac{\partial \rho}{\partial t} + \frac{\partial \rho u}{\partial x} = 0. \tag{41}$$

Substituting $\rho = \bar{\rho} + \rho'$ and $\rho u = (\bar{\rho} + \rho')(\bar{u} + u') = \bar{\rho}\bar{u} + \rho'\bar{u} + \bar{\rho}u' + \rho' u'$ into equation (41) yields;

$$\frac{\partial \bar{\rho}}{\partial t} + \frac{\partial \rho'}{\partial t} + \frac{\partial \bar{\rho}\bar{u}}{\partial x} + \frac{\partial \rho'\bar{u}}{\partial x} + \frac{\partial \bar{\rho}u'}{\partial x} + \frac{\partial \rho' u'}{\partial x} = 0. \tag{42}$$

Taking the time average of equation (42) provides;

$$\frac{\overline{\partial \bar{\rho}}}{\partial t} + \frac{\overline{\partial \rho'}}{\partial t} + \frac{\overline{\partial \bar{\rho}\bar{u}}}{\partial x} + \frac{\overline{\partial \rho'\bar{u}}}{\partial x} + \frac{\overline{\partial \bar{\rho}u'}}{\partial x} + \frac{\overline{\partial \rho' u'}}{\partial x} = 0,$$

where the only non-zero terms are;

$$\frac{\overline{\partial \bar{\rho}}}{\partial t} + \frac{\overline{\partial \bar{\rho}\bar{u}}}{\partial x} + \frac{\overline{\partial \rho' u'}}{\partial x} = 0$$

or since $\bar{\bar{f}} = \bar{f}$ (see Ref. 5 or Ref. 10 for a more complete derivation) this is the same as;

$$\frac{\partial \bar{\rho}}{\partial t} + \frac{\partial \bar{\rho}\bar{u}}{\partial x} + \frac{\partial \overline{\rho' u'}}{\partial x} = 0. \qquad (43)$$

Comparing equation (43) and (41) reveals that the continuity equation using the original variables differs from the continuity equation using the time-averaged variables only by the addition of a function of $\overline{\rho' u'}$. The Reynolds-averaged form of the momentum equation and the energy equation follow a similar procedure. In each case the Reynolds-averaged equations using time-averaged variables are equal to the original equations plus some terms containing time-averaged products of fluctuating variables. For example, the momentum equation in the x direction for two-dimensional flow may be written as[11];

$$\frac{\partial}{\partial t}(\bar{\rho}\bar{u} + \overline{\rho' u'}) + \frac{\partial}{\partial x}(\bar{\rho}\bar{u}\bar{u} + \bar{u}\overline{\rho' u'}) + \frac{\partial}{\partial y}(\bar{\rho}\bar{u}\bar{v} + \bar{u}\overline{\rho' v'}) =$$

$$-\frac{\partial \bar{p}}{\partial x} + \frac{\partial}{\partial x}\{\mu[2\frac{\partial \bar{u}}{\partial x} - (2/3)(\frac{\partial \bar{u}}{\partial x} + \frac{\partial \bar{v}}{\partial y})] - \bar{u}\overline{\rho' u'} - \bar{\rho}\overline{u' u'}$$

$$- \overline{\rho' u' u'}\} + \frac{\partial}{\partial y}[\mu(\frac{\partial \bar{u}}{\partial y} + \frac{\partial \bar{v}}{\partial x}) - \bar{v}\overline{\rho' u'} - \bar{\rho}\overline{u' v'} - \overline{\rho' u' v'}]. \qquad (44)$$

Using the same definition for $\bar{\tau}_{xx}$ as for τ_{xx} (equation (14)) the right-hand side of equation (44) becomes;

$$\frac{\partial}{\partial x}(\bar{\tau}_{xx} - \bar{u}\overline{\rho' u'} - \bar{\rho}\overline{u' u'} - \overline{\rho' u' u'}) +$$

$$\frac{\partial}{\partial y}(\bar{\tau}_{xy} - \bar{v}\overline{\rho' u'} - \bar{\rho}\overline{u' v'} - \overline{\rho' u' v'}).$$

The time averages of the fluctuating variables are said to look like stress terms. $-\bar{\rho}\overline{u' v'}$ and $-\bar{\rho}\overline{u' u'}$ are specifically identified as "Reynolds stresses." Note that ρ is not time averaged in this definition because the classical definition for Reynolds stresses was derived for incompressible flow.[10] These apparent stresses provide a measure of the momentum transport due to the turbulent motions in the boundary layer. Applying the same averaging techniques to the energy equation produces apparent heat-flux terms[5] ($\overline{\rho' T' u'}$, $\overline{\rho' T' u'}$, etc.).

The time averaging process provides equations for the large scale features of the flow but at the expense of introducing several additional unknowns. Incompressible analysis greatly simplifies the Reynolds averaged equations because all terms containing ρ' would vanish. Compressible flow equations are simplified somewhat by using order-of-magnitude arguments.[1,5] In recent years it has become popular to develop Reynolds-averaged equations using mass-weighted averaging for the flow and thermal variables. This approach produces relatively simple momentum and energy equations without making simplifying assumptions. However, much more complex expressions are obtained for the stresses, and order-of-magnitude arguments are required in order to evaluate them. Ref. 5 provides a good comparison between classical time-averaging and mass-averaging.

Determining what to do about the remaining new terms, and how to do it is referred to as the "closure problem" for Reynolds-averaged Navier-Stokes solutions. In the development of the original Navier-Stokes equations researchers looked to the properties of the fluid for closure information (e.g. the perfect gas relationships). The search for ways to evaluate the products of the fluctuating properties is referred to as "turbulence modeling" and relies heavily on experimental observations.

Many different turbulence models with wide degrees of complexity have been proposed. Probably the simplest, and the only one to be discussed here, is based on the Boussinesq[1,5,10] assumption that the Reynolds stresses are related to the laminar stress terms through an "eddy" viscosity term (ϵ).

$$-\rho\overline{u'v'} = \epsilon\left(\frac{\partial\bar{u}}{\partial y} + \frac{\partial\bar{v}}{\partial x}\right)$$

$$-\rho\overline{u'u'} = \epsilon\left[2\frac{\partial\bar{u}}{\partial x} - (2/3)\left(\frac{\partial\bar{u}}{\partial x} + \frac{\partial\bar{v}}{\partial y}\right)\right]$$

$$-\rho\overline{v'v'} = \epsilon\left[2\frac{\partial\bar{v}}{\partial y} - (2/3)\left(\frac{\partial\bar{u}}{\partial x} + \frac{\partial\bar{v}}{\partial y}\right)\right]$$

Note that the value for ϵ may be different in each equation; however, the convention is to assume they are equivalent. The local mean density is used for the eddy viscosity definition. The other fluctuating terms

are assumed to be small and are neglected in the definition of the turbulent shear stress. These simplifications appear to work well for attached boundary layers at Mach numbers up to 5[5]. The obvious advantage of this definition is that the total viscosity is then the sum of the thermodynamic viscosity μ and the eddy viscosity ϵ.

In a similar manner an "eddy" conductivity (k_t) may be defined to approximate the turbulence effects on the energy equation;

$$-\rho c_p \overline{v' T'} = k_t \frac{\partial \bar{T}}{\partial y}$$

Fortunately, experiment has shown that the eddy conductivity can be related to the eddy viscosity through the turbulent Prandtl number (Pr_t);[1,5]

$$k_t = c_p \epsilon / Pr_t .$$

Where Pr_t is assumed to be a constant with a value near 1.0. Closure of the Reynolds averaged Navier-Stokes equations now depends solely on the evaluation of the eddy-viscosity. Unfortunately the eddy-viscosity is not a simple physical property of the fluid as is thermodynamic viscosity μ.

Algebraic Eddy Viscosity Model

Algebraic or zero-equation (meaning no partial differential equations) models for ϵ invariably incorporate the Prandtl mixing length assumption;

$$\epsilon = \rho \ell^2 \left| \frac{\partial \hat{u}}{\partial \hat{y}} \right| .$$

Where ℓ is the transverse distance over which a turbulent structure maintains its original momentum. $\hat{u}$ is the velocity in the primary flow direction ($\hat{x}$), and $\hat{y}$ is transverse to $\hat{u}$. The remainder of this discussion will be on the Baldwin-Lomax[11] model used in this study. This description is for two-dimensional flow and the variables $\hat{u}$, $\hat{v}$, $\hat{x}$, and $\hat{y}$ are as defined above but the $\hat{}$ will be dropped.

The Baldwin-Lomax model is a two-layer algebraic model with an intermittency factor. Two-layer means that there are two separate equations; one for the inner layer that forces the eddy viscosity to approach zero at the wall, and another equation for the remainder of the boundary layer. The intermittency factor is an experimentally derived expression that accounts for the decreasing frequency of encountering turbulent flow structures in the flow outside of the boundary layer.

An eddy-viscosity coefficient is defined at each x location. The equation for the inner eddy-viscosity (ϵ_i) is;

$$\epsilon_i = \rho \, \ell^2 \, |\omega| . \tag{45}$$

Where

$$\ell = k \, y \, D,$$

k is the von Karman constant = 0.40

D is the van Driest damping function;

$$D = 1 - e^{(-y^+/A^+)},$$

A^+ is a sublayer constant = 26,

$$y^+ = y \, (\frac{(\rho\tau)^{1/2}}{\mu})|_w$$ (subscript w refers to the solid surface),

$$|\omega| = |(\frac{\partial v}{\partial x} - \frac{\partial u}{\partial y})| .$$

The von Karman constant provides the proper scaling for ℓ near the solid surface. The van Driest function provides for the transition from the viscous sublayer to the fully developed turbulent outer region. Therefore, ℓ varies from zero at the surface to essentially a linear function at large distances from the surface. $|\omega|$ is the magnitude of the vorticity which is typically very large near the surface, then decreases rapidly through the boundary layer.

The equation for the outer eddy viscosity (ϵ_o) for attached flow over a solid surface is;

$$\epsilon_o = \rho \, K \, C_{cp} \, F_{wake} \, F_{kleb} \tag{46}$$

where,

K is the Clauser function = 0.0168,

C_{cp} = 1.6,

$$F_{wake} = Y_{max} F_{max}. \quad (47)$$

The Clauser constant is related to the Reynolds number based on boundary layer thickness[5] and C_{cp} is a constant applied to this method to match the Cebeci-Smith[12] results. F_{max} is determined from the equation;

$$F(y) = y\,|\omega|\,D$$

by locating the y value at which F(y) is a maximum for a given x location. Y_{max} is the value of y that produces F_{max}. This F(y) function is reported[11] to be a much more reliable indicator than trying to find the edge of the boundary layer as in previous (e.g. Cebeci-Smith[12]) methods.

The edge of the boundary layer is not a clearly defined location. The random encounter with turbulence above the mean edge of the boundary layer is referred to as intermittency. Intermittency effects are accounted for by the Klebanoff intermittency factor (F_{kleb});

$$F_{kleb} = [\,1. + 5.5(C_{kleb}\,\frac{y}{Y_{max}})^6\,]^{-1},$$

where C_{kleb} = 0.30. F_{kleb} is a function such that the value of F_{kleb} is near 1 at small values of y but diminishes rapidly as y extends beyond the edge of the boundary layer.

With a slightly different definition for F_{wake} the outer eddy viscosity formulation is reported[11] to be valid for separated flow and wakes. The separated-flow/wake formulation for F_{wake} is:

$$F_{wake} = (C_{wk}\,Y_{max}\,U^2_{dif})/F_{max}, \quad (48)$$

where

C_{wk} is another empirical constant = 0.25,

$$U_{dif} = (u^2 + v^2)^{1/2}_{max} - (u^2 + v^2)^{1/2}_{min},$$

and F_{max} is as defined above. For separated flow over a solid surface the second term for U_{dif} is zero, and for wake flow D = 1 in the F_{max} equation. To avoid having to locate the point of separation, if any, Ref. 11 suggests calculating F_{wake} both ways (equations (47) and (48)) and using the smallest value.

For a given x location, both an inner and an outer eddy viscosity coefficient have been defined (equations (45) and (46) respectively). Obviously both equations will provide a value for ϵ for any value of y. Ref. 11 suggests calculating both values and switching from using the inner value (ϵ_i) to the outer (ϵ_o) value at the smallest value of y for which $\epsilon_i > \epsilon_o$. Note that this criterion is not the same as simply choosing the smaller of the two values.

It is important to remember that the eddy viscosity model coefficients are based on experimental observations, usually on flat plates and at subsonic Mach numbers. The values for the constants provided are all subject to debate,[13,14,15] particularly in regions of high pressure gradients, wakes, and at high transonic or supersonic Mach numbers. Also, many researchers are very critical of using the algebraic equation model for flow conditions that are not fully attached.[16,17,18]

The reason for emphasis on the Baldwin-Lomax procedure and its inherent deficiencies will become apparent in the next section where a modification of the Baldwin-Lomax approach that allows solutions for flow with massive shock-induced separation is described. First, however, a discussion on boundary conditions and computational grids is necessary.

Boundary Conditions

A discussion on boundary conditions should probably begin with a discussion on existence, uniqueness and "well-posedness." Ref. 15 points out that there is no rigorous mathematical theorem to define the criteria to ensure existence and uniqueness of solutions for the Navier-Stokes equations. Ref. 7 points out that uniqueness is particularly

uncertain, and refers to stall hysteresis and other examples where different flow conditions may exist for identical boundary conditions. Existence of solutions appears to be somewhat less of a problem.[7,19,20]

A problem is said to be well-posed if any small change in the boundary/initial conditions produces a corresponding small change in the solution.[19] Ref. 20 suggests that, for the one-dimensional, incompressible form of the Navier-Stokes equations, well-posed conditions are (1) known fixed initial conditions for each variable, and (2) Dirichlet boundary conditions. Dirichlet boundary conditions are one of the three classes of boundary conditions defined in Ref. 2 as:

Dirichlet - Values for the variables are specified on the boundary.

Neumann - The normal derivative of the variable is specified on the boundary.

Robins (or mixed) - A linear combination of Dirichlet and Neumann boundary conditions.

Solid surface boundary conditions for the momentum equation variables (u, v) are exceedingly simple; velocity relative to the surface equals zero. The energy equation variable (e) is usually determined by computing the temperature at the surface, then

$$e_w = C_v T_w$$

where the subscript w refers to the wall or surface. Remember that the velocity at the wall is zero. The two most common surface conditions for temperature are:

$$T_w = \text{constant}$$

or

$$\left(\frac{\partial T}{\partial y}\right)_w = 0.$$

Classical heat transfer equations could be employed for more difficult cases. Equilibrium temperature is reached very quickly for metallic models in continuous flow wind tunnels. Therefore, the solution procedure discussed in this report uses a turbulent flow recovery factor to estimate wall temperature.[10]

$$T_w = T_\infty [1 + \frac{\gamma - 1}{2} M_\infty^2 \, Pr^{1/3}]$$

The continuity equation variable (ρ) remains to be defined at the solid surface. This is usually accomplished by applying the experimentally observed characteristic of the pressure gradient through the boundary layer perpendicular to the surface;

$$(\frac{\partial p}{\partial y})_w = 0. \tag{49}$$

(Ref. 2 obtains this result by examining the momentum equation normal to the surface.) Using the equation of state in equation (49) provides a finite difference approximation for density at the wall;

$$\rho_w = \rho_2 \, (\frac{T_2}{T_w}).$$

The subscript 2 refers to the first grid level above the surface. Note that ρ_w is a compatibility condition, not a true boundary condition and the smaller the first grid step, the better this approximation.

A "C" type computational grid (Figure 1) was used for the solutions in this study (grid generation is discussed in the next part). As a result, there is a branch cut extending from the trailing edge of the airfoil to the downstream boundary. The upper and lower parts of the grid have common points along the cut line. Values of the flow variables along the cut line are defined as the average of the value at the first level above and the first level below the cut line.

The most difficult and controversial boundary conditions arise at the "far-field" boundaries. Problems occur because the computational domain for the numerical solution is necessarily limited in both space and time. For example, an F-15 flying at 30,000 feet has a far-field boundary (the earth) about 500 fuselage lengths away. The most generous numerical boundary would have to be an order of magnitude or more smaller. The task then is to devise physically accurate, stable and, hopefully, uncomplicated boundary conditions for the flow variables at these artificial boundaries.

In supersonic flow disturbances cannot propagate upstream from the body, therefore, boundaries with flow into the computational domain must

be at free stream conditions (e.g., $\rho = \rho_\infty$,etc.). Likewise, disturbances downstream of the body cannot propagate upstream to influence the flow over the body. As a result, the simple procedure of extrapolating the values of the variables from the interior of the domain to the downstream boundary provides satisfactory results.

Subsonic flow conditions present the most difficulties for estimating the proper values for the flow variables at the far field computational boundaries. Recent literature[16] focuses on three primary approaches. The most complex of these involves defining the primary flow variables in terms of characteristic variables derived from two-dimensional, inviscid equations.[21] A form of this approach, referred to as Riemann invariant,[22] is used to define the upstream boundary conditions in the code used for this investigation. Table 1 provides a summary of the Riemann invariant procedure. Next in level of complexity is the non-reflecting boundary conditions.[23] As the name implies, the objective is to allow disturbances produced in the solution domain to "pass through" the boundary and not be reflected back to contaminate the solution. This procedure was not used in the current study, and the interested reader is referred to Ref. 23. The simplest boundary conditions use free stream values for the primary variables at the upstream boundary, and "no-change" conditions at the downstream boundary. No-change simply means that the value of the variable at the boundary equals the value at the first computed grid point inside the boundary. This approach over-specifies the boundary conditions, but produces reasonable results[24] when the boundary is located sufficiently far from the body. Ref. 24 provides a good summary of the three approaches discussed above and compares the results of applying each for the solution of flow around a cylinder.

With the numerical boundaries at sufficiently large distances from the body (say 50 body lengths), the effects of the type of boundary condition applied would be expected to vanish. However, computer memory, run times and the error introduced by highly stretched grids put severe constraints on practical locations for the far field boundaries. The

Riemann invariant approach would seem to provide a more physically accurate representation. Ref. 25 claims very good results with such an approach for a finite volume solver. However Shang[24] observed little or no difference between the characteristic method, the non-reflecting method or the simple free stream and no-change approach when used with an explicit finite difference solver on flow over a cylinder. This author has used both the Riemann invariant and the free stream/no-change boundary conditions for flow over an airfoil with no observable differences. Both this study and Ref. 24 obtained viscous flow solutions with far-field boundaries at about 10 reference body lengths, and both used a similar explicit finite difference code.

The selection of far field locations and the boundary conditions to be applied are still an inexact, controversial, and continuously evolving art. The results provided in this report used the Reimann invariant boundary conditions for inflow (upstream) boundaries, and the no-change conditions for outflow (downstream) boundaries. These boundary conditions were chosen because they seem more physically proper and because other government and industry personnel conducting similar studies have had good success (private conversations). Visbal[26] obtained good results for transonic flow over airfoils with free stream far-field boundary conditions when the boundary was sufficiently far away. The far-field boundaries for results presented in this study were located at approximately 15 chord lengths away from the airfoil.

Computational Grid

Finite difference solutions of the partial differential equations governing fluid flow about arbitrary bodies require the development of a computational grid around the body. A grid system that conforms to the shape of the body at the surface has the very important advantages of simplifying the partial differential equation solution technique and simplifying the satisfaction of the surface boundary conditions. The character of the entire flow field is determined in the high gradient regions near the body. Therefore, the development of a body-conforming

coordinate system and computational grid is a very important first step in the numerical solution of fluid flow problems.

Algebraic grid generation techniques have been used for some applications and have the advantage of being relatively simple and fast.[27] However, the most popular techniques use the solution of partial differential equations (PDE). Procedures exist that solve elliptic, hyperbolic and parabolic PDEs. Elliptic routines are most often used and probably are more generally applicable to a wider range of problems. Hyperbolic routines are relatively fast and simple, but are not easily adapted to physical constraints in the computational domain (such as internal flows or multiple bodies).[28] Parabolic routines have been recently developed and show some promise.[29] The PDE methods attempt to produce nearly orthogonal grids with assurance of no crossover of adjacent grid lines.

A hyperbolic grid generation routine was chosen for this study because it is quite fast, provides nearly orthogonal grids and has good user control of the grid spacings. The routine appears to work well for generating a grid around two-dimensional bodies when there are no other physical constraints within the domain of the grid. The actual grid generation starts at the body at user defined locations and marches out to an outer boundary.

The core of the program was adapted from the O-grid procedure described by Steger and Chaussee.[28] That procedure was modified for this study by including additional dissipation terms and by changing the form of the dissipation described. The modifications necessary to produce a C-type grid are also described and an example is provided.

It is desirable that the distribution of points around the body be second-order smooth.[27] Since most bodies are defined with a somewhat random distribution of points, a routine was added to redefine the coordinates in a smooth distribution.[30] This routine also allows selective clustering of grid points in regions of high gradients.

In the grid generation algorithm developed by Steger and Chaussee,[28] definitions of grid orthogonality and the transformation Jacobian were chosen to devise a scheme mapping x,y into ξ,η:

$$x_\xi x_\eta + y_\xi y_\eta = 0 \tag{50}$$

$$x_\xi y_\eta - x_\eta y_\xi = 1/J \tag{51}$$

Note that by the definition of the Jacobian, cell areas in physical and computational domains can be written;

$$dA = dxdy = (1/J)\, d\xi d\eta$$

Numerically the grid spacings in the transformed plane, $\Delta\xi = \Delta\eta = 1$, so the inverse Jacobian approximates the physical cell area. Equations (50) and (51) are locally linearized using;

$$x = \overset{\bullet}{x} + \Delta x$$

$$y = \overset{\bullet}{y} + \Delta y$$

where $\overset{\bullet}{x}, \overset{\bullet}{y}$ is a nearby location. The linearized set of equations become (after some algebraic manipulation)

$$\begin{bmatrix} \overset{\bullet}{x}_\eta & \overset{\bullet}{y}_\eta \\ \overset{\bullet}{y}_\eta & -\overset{\bullet}{x}_\eta \end{bmatrix} \begin{bmatrix} x \\ y \end{bmatrix}_\xi + \begin{bmatrix} \overset{\bullet}{x}_\xi & \overset{\bullet}{y}_\xi \\ -\overset{\bullet}{y}_\xi & \overset{\bullet}{x}_\xi \end{bmatrix} \begin{bmatrix} x \\ y \end{bmatrix}_\eta = \begin{bmatrix} 0 \\ A+\overset{\bullet}{A} \end{bmatrix}$$

or, substituting symbols for the matrices and vectors;

$$C\,\vec{R}_\xi + B\,\vec{R}_\eta = \vec{f} \tag{52}$$

The specific numerical procedure for solving equation (52) depends on the class of equation (i.e., elliptic, parabolic, or hyperbolic). The class can be determined by inspecting $B^{-1}C$.

$$B^{-1}C = 1/\overset{\bullet}{J} \begin{bmatrix} \overset{\bullet}{X}_\xi \overset{\bullet}{X}_\eta - \overset{\bullet}{Y}_\xi \overset{\bullet}{Y}_\eta & \overset{\bullet}{X}_\xi \overset{\bullet}{Y}_\eta + \overset{\bullet}{Y}_\xi \overset{\bullet}{X}_\eta \\ \overset{\bullet}{X}_\eta \overset{\bullet}{Y}_\xi + \overset{\bullet}{Y}_\eta \overset{\bullet}{X}_\xi & \overset{\bullet}{Y}_\xi \overset{\bullet}{Y}_\eta - \overset{\bullet}{X}_\eta \overset{\bullet}{X}_\xi \end{bmatrix}$$

where,

$$J = X_\xi^{2} + Y_\xi^{2}$$

Since $B^{-1}C$ is symmetric, it has real eigenvalues, specifically;

$$\lambda_{1,2} = \pm 1/J \sqrt{(X_\xi X_\eta - Y_\xi Y_\eta)^2 + (X_\xi Y_\eta + Y_\xi X_\eta)^2}$$

This indicates that the system is hyperbolic and can be marched in the η direction in a time-like manner. The finite difference solution scheme chosen to approximate equation (52) is centrally differenced in ξ and backward differenced in η. The scheme can be written as;

$$[I + B^{-1}C\,\delta_\xi]\,\vec{R}_{i,j+1} = \vec{R}_{i,j} + B^{-1}\,\vec{f}_{i,j+1} + \sigma\,(\hat{\nabla}_i\,\hat{\Delta}_i)^2\,\vec{R}_{i,j}$$

where δ_ξ represents a central difference in the ξ direction, i represents the index in the ξ direction, and j represents the index in the η direction. $\vec{f}_{j+1}$ is assumed to be known at the j level by a process shown below, and $\sigma\,(\hat{\nabla}_i\,\hat{\Delta}_i)^2\,\vec{R}_{i,j}$ is an added fourth order dissipation term in ξ to aid in stability.[31]

Typically x_ξ, and y_x are approximated as;

$$x_\xi = (x_{i+1,j} - x_{i-1,j})/2$$

$$y_\xi = (y_{i+1,j} - y_{i-1,j})/2$$

While x_η and y_η are extracted from the nonlinear differential equations (50) and (51).

$$x_\eta = (-y_\xi A)/J, \qquad y_\eta = (x_\xi A)/J,$$

This allows the nonlinearity to be maintained.

As mentioned before, the cell areas at the j and j+1 levels are assumed to be known. This can be accomplished in any number of ways. Steger and Chaussee[28] construct polar grids about two individual circles whose circumference is the arc length of the body to be grided. The grids on these two circles have the same spacing in the radial direction

but differ in grid spacing in the circumferential direction. One circle has points placed in equally spaced increments around the circumference and the other circle has the same spacing as the point distribution over the body. Cell areas are extracted from these polar grids such that when near the body, cell areas are calculated using the non-uniform distribution of points, and when far from the body, areas from the uniform distributed circle are used. A smooth function transitions from the inner areas to the far-field areas at a user defined rate.

The solution algorithm proposed for these equations exhibited difficulties for geometries with slope discontinuities and regions of reverse (concave) curvature. Discontinuities propagated into the grid interior with undesirable results. Drawing from experience in other hyperbolic systems it was postulated that these problems could be circumvented without drastically compromising orthogonality by carefully including other forms of dissipation. Using the analogy between marching in time and marching in η, a time-like dissipation was added to insure smoothness. To accomplish this task, a more general class of integration in η was chosen:

$$\frac{\vec{R}_{j+1} - \vec{R}_j}{\Delta\eta} = (1-\alpha)\left(\frac{\partial R}{\partial \eta}\right)_j + \alpha\left(\frac{\partial R}{\partial \eta}\right)_{j+1}$$

When $\alpha = 1$, the original backward differenced scheme is obtained. The numerical error term for this scheme is

$$(1/2)\ (1-2\alpha)\ \Delta\eta\ \frac{\partial^2 R}{\partial \eta^2} + \text{higher order terms.}$$

Note that for $\alpha = 1/2$ the integration is a trapezoidal type and is formally second-order in η. For $\alpha > 1/2$ the error term has a dissipative effect in the η direction. Rewriting the algorithm in delta form, such that increments in $\vec{R}$ ($\Delta\vec{R} = \vec{R}_{j+1} - \vec{R}_j$) may be determined, the algorithm becomes:

$$[I + \alpha\, B^{-1} C\, \delta_\xi](\vec{R}_{j+1} - \vec{R}_j) = B_j^{-1}(\alpha A^0_{j+1} + (1-\alpha)A_j) +$$

$$\sigma(\hat{\nabla}_i \hat{\Delta}_i)^2 \vec{R}_j .$$

Adding second-order implicit dissipation to this algorithm serves to augment the amount of explicit dissipation that may be added before degrading the accuracy of the method. Therefore, the final form of the algorithm with both implicit and explicit dissipation, and the "alpha" parameter, α is:

$$[I + \sigma_1 (\nabla_i \Delta_i) + \alpha B^{-1} C \delta_\xi](\vec{R}_{j+1} - \vec{R}_j) =$$

$$B^{-1}(\alpha A^0_{j+1} + (1-\alpha)A_j) + \sigma_2 (\hat{\nabla}_i \hat{\Delta}_i)^2 \vec{R}_j .$$

σ_1 is the implicit dissipation coefficient and σ_2 is the explicit dissipation coefficient.

The marching algorithm allowed by the hyperbolic form of the equations provides an efficient means for constructing a computational grid. A grid solution begins by initializing the variables for grid stretching, dissipation coefficients, α, and reading in the user defined body coordinates. Table 2 provides an example cf the values of the parameters used to produce the computational grids in this study. The marching procedure in the η direction (increasing j) consisted of four steps. First, the areas at the j+1 level were approximated by the method described above. Then a system of equations was set up to determine the increments in x and y. This resulted in a 2x2 block tridiagonal matrix to be solved. The increments in x and y were then known at the j level for each ξ (i) station, and grid points at the j+1 level were computed using these increments. The process was repeated until the maximum grid level was reached at the outer boundary.

O-type computational grids are widely used for a variety of solution procedures (Euler and full potential for example). For viscous flow applications, however, a C-type grid is preferred. The viscous flow characteristics around an airfoil and the resulting wake area behind the airfoil require fine grid spacings close to the body and in the wake.

The most obvious change required in converting an O-grid routine to a C-grid routine is the establishment of a downstream boundary spacing procedure (boundary condition). A separate subroutine was created to compute the downstream boundary spacings. x is fixed at the maximum

(downstream) value and y is incremented as $\pm \Delta\vec{R}$, the step size in the normal (η) direction. The terms that defined the periodic nature of the O-type grid were eliminated from the tridiagonal matrix. Figure 1 shows a comparison of an O-type and a C-type grid around the NLR 7301 airfoil analyzed in this study.

The hyperbolic grid generating procedure is very fast (a few seconds on a PRIME 750) and provides a grid pattern with a lot of user control. The routine is tolerant to variations of all input parameters (robust) except for the parameter that controls the transition to equal cell areas. Rapid changes in grid spacing around the body or concave regions may cause a shock-like discontinuity to develop and propagate through the grid. Tolerance to these conditions may be improved (at some sacrifice in orthogonality) by changing σ_1, σ_2, or a and/or by adding or deleting grid points along the body.

II. APPLICATION TO A SUPERCRITICAL AIRFOIL

Current State of the Art

The objective of this Navier-Stokes work was to compute the two-dimensional, steady-state flow over a 16.5% thick supercritical airfoil (NLR 7301) at a Mach number of 0.807 and an angle of attack of 0.36 degrees. Reynolds number based on the chord length ranged from 3 to 12 x 10^6 and boundary layer transition from laminar to turbulent occurred naturally at approximately 10 percent chord. At these conditions there is a strong shock on both the upper and lower surfaces with separated flow extending from the shocks to the trailing edge (Figure 2). These conditions present a severe test case for computational methods. Successful solutions (solutions that accurately match experimental data) for flow conditions with strong shocks and extensive separation are rare. Poor agreement between experimental and computational results may be caused by such things as inadequate computational grids, improper boundary conditions (which includes wind tunnel wall effects) and invalid turbulence models.

Computational grids with as few as 5,400 points (135 x 40) to as many as 50,000 points (500 x 100) were used in this study. Even a two-block grid was used where a separate grid block extended from the blunt trailing edge of the model to the downstream boundary. Far-field boundaries as near as five chord lengths to as far as 25 chord lengths were examined (there was no attempt to model the wind tunnel walls). The initial grid spacing from the surface ranged from 0.00005 to 0.001 chord lengths. Riemann invariant, non-reflective and free stream/no-change farfield boundary conditions were all tried at some point in the study. The net result of these attempts was that, only at Mach = 0.752 and below could a solution that matched the experimental data[32] be obtained

using the basic equations and procedures described in the previous section. Figure 3 shows a typical Mach = 0.752 comparison of the pressure coefficients from the MacCormack explicit code used in this study ("Shang" code) and the NASA/Ames ARC2D[33] code; an implicit, thin-layer procedure. The ARC2D code is widely used in government and industry and was used in this study as a "control" code for the current study.

At M = 0.807 the computational solution did not match experimental data for any of the computational domains and boundary conditions attempted. There were two "solutions" for the Mach = 0.807 condition. An attached flow solution, which occurred when the eddy viscosity was allowed to become large (the attached-flow equation for F_{wake}(47)), and an oscillatory solution when eddy viscosity was kept small (the separated-flow/wake equation for F_{wake}(48)). The oscillatory solution was also observed with the ARC2D code, which employs the Baldwin-Lomax turbulence model. Figure 4 shows how the lift coefficient varied with increasing iterations for both ARC2D and the Shang code. (The shape of the oscillatory lift curve was sensitive to grids, boundary conditions and other factors. Comparisons with ARC2D results are provided only to show that the problems are not unique to the Shang code.)

Oscillatory solutions appeared to alternate between being attached on one surface and separated from the other, then reversing. This apparent periodic variation in the lift coefficient was observed even though the solutions were not run time-accurate. A similar periodic phenomenon has been observed experimentally on an 18% thick circular arc airfoil,[34] however, no such oscillations were observed during the test of Ref. 32 (according to private conversations with the author). Lift variations of the magnitude indicated by Figure 4 could have hardly gone unnoticed.

Researchers familiar with algebraic turbulence models would probably not be surprised by the poor results at Mach = 0.807. Indeed, every analysis of transonic turbulent flow prediction consulted (cf. Refs. 16,17,18) emphasized the inadequacies of turbulence models for separated flow. This study had to this point only succeeded in reinforcing those assessments. Some success in computing axisymmetric flow

with local separation had been reported by using a "hybrid" eddy-viscosity/Reynolds shear-stress turbulence model.[35] That procedure was incorporated into the Shang code in place of the Baldwin-Lomax model, but the results were not noticeably better than the previous results. Of course we must always be skeptical of results obtained from trying to duplicate another author's procedure with only limited information.

Analysis of the Algebraic Turbulence Model

Some insight into the oscillating solution problem was gained by looking at the results for Mach = 0.75 on a 340 x 85 grid, and with the Baldwin-Lomax model as described in Ref. 11. That is, F_{wake} over the body was chosen as the minimum of;

$$F_{wake} = (Y_{max} F_{max}),$$

or,

$$F_{wake} = (C_{wk}\, Y_{max}\, U_{dif}^2)/F_{max}.$$

The convergence proceeded rather rapidly; however, the lift and drag never reached a constant value (Figure 5). There was evidence of small oscillations, primarily in the shock location on the upper surface (Figure 6). A change was made in the program so that F_{wake} was defined only as $(Y_{max}\, F_{max})$ over the body surface, and the oscillations immediately disappeared. Apparently the increase in dissipation from the greater eddy viscosity on the upper surface was sufficient to fix the shock location and permit convergence.

The ineffectiveness of changes in the computational domain, the acknowledged inadequacies of simple eddy-viscosity models, and the above results at M = 0.75, suggested that the key to converged solutions for the Mach = 0.807 condition might lie in establishing the proper level of eddy-viscosity for the separated region aft of the shocks. A more detailed investigation of the key parameters in the Baldwin-Lomax model was initiated. In the attached-flow formulation (equation (47)), F_{wake} outside of the inner layer is essentially a function of Y_{max} and $|\omega|$.

$$F_{wake} \sim Y^2_{max} |\omega|_{Y_{max}}$$

Therefore, when the boundary layer is thin, Y_{max} is small and thus F_{wake} is small. In separated flow behind a shock, however, the boundary layer thickens rapidly, Y_{max} gets large, and F_{wake} increases as the square of Y_{max} (Figure 7). The resulting large values for eddy viscosity produce large amounts of dissipation in the separated flow region and suppress any tendency for separation. This results in the strong attached-flow convergence for the $M = 0.752$ and $M = 0.807$ (Figure 8).

The separated-flow/wake formulation for F_{wake}, (equation (48)), outside of the inner layer is essentially;

$$F_{wake} \sim C_{wk} U^2_{dif}/|\omega|_{Y_{max}}; \qquad C_{wk} = \text{constant}.$$

Notice that boundary-layer thickness does not appear in the expression. Rather, F_{wake} varies as the square of the maximum velocity at the x location of interest. Figure 9 shows U^2_{dif}, $|\omega|_{Y_{max}}$ and F_{wake} for a typical oscillatory result for $M = 0.807$. U^2_{dif} decreases rapidly aft of the shock (approximately 60 percent chord). Since F_{wake} is a function of the square of U_{dif}, changes in velocity would tend to have a large and immediate effect on F_{wake}, and thus, eddy-viscosity.

Consider the following hypothesis: Some perturbation causes the shock wave on one surface to become slightly stronger which reduces the velocity downstream of the shock. The vorticity, ω, at Y_{max} may also decrease, but since F_{wake} is proportional to the square of U_{dif}, the immediate effect is that eddy-viscosity is reduced. The resulting decrease in dissipation aft of the shock produces a larger separated flow region, drives the shock farther forward, and it becomes still stronger. This produces an even lower U_{dif}, and the process continues. Eventually something (change in circulation, vorticity, etc.) stops the forward movement and the shock starts to move aft and weaken. Again,

the process is self-sustaining because U_{dif} increases, eddy-viscosity gets larger, and the separated region decreases. The shock continues to move aft until the flow is fully attached on that surface, and then the cycle repeats.

This type of self-sustained, oscillatory behavior was observed for all computations that had strong shocks with massive separation on both upper and lower surfaces. However, it was not obvious during the experiment; at least not to the magnitude indicated by the computed results. Obviously, something was missing in the computed results, and all indications were that the turbulence model was not providing correct levels of eddy-viscosity. Something was needed in the definition of F_{wake} that defeated the self-sustaining movement of the shock wave and the corresponding change in the separated flow region.

Modifications to the Algebraic Turbulence Model

Examination of the flow in the separated region (Figure 10), revealed a reversed flow region near the body, and a high velocity gradient region at the outer edge of the separated flow. An attempt was made to treat these two regions with separate, attached-flow turbulence models by applying equation (47) to each region independently. That approach proved unsuccessful because the eddy-viscosity became so large that the reversed flow region was completely suppressed. Another approach based on the separated-flow/wake formulation (equation (48)) for F_{wake} in the separated region, plus a weighted function of the height of the reversed flow region to represent the additional dissipation needed, was developed. The resulting equation may be written as;

$$F_{wake} = \frac{C_{wk}\, Y_{max}\, U_{dif}^2}{F_{max}} + (D_{wk} Y_0)\, \frac{C_{wk}\, Y_{max}\, U_{dif}^2}{F_{max}}$$

The last term is the additional, weighted dissipation, and is proportional to the height (Y_0) of the reversed flow region.

The original equation for F_{wake} can be retained if a new, variable coefficient is defined as;

$$C_{wks} = C_{wk}(D_{wk}\ Y_0 + 1).$$

Where,

Y_0 is the height of the reverse flow region,

D_{wk} is a weighting function whose value is to be determined.

C_{wks} was substituted for C_{wk} in the equation for F_{wake} and was computed at each x location for each iteration. The value of C_{wks} changes in direct proportion to the height of the reverse flow region, which provides the additional dissipation necessary to counteract the influence of U_{dif} changes.

The new parameter, D_{wk}, was evaluated to determine the magnitude needed, and to assess its effect on the solution. Values from 20 to 120 were used. Figure 11 shows the effect on C_L of the different values for D_{wk}. As would be expected, the larger values of D_{wk} provide large eddy-viscosity and produce results that approach the solutions obtained with the attached flow equation for F_{wake}. The smaller values of D_{wk} provide solutions that show signs of the oscillations observed with the original separated-flow/wake equation for F_{wake}. Figure 11 indicates that the lift approaches a minimum value at about $D_{wk} = 60$, and oscillates about this mean value at lower levels of D_{wk}. Unfortunately, drag (Figure 12) does not seem to approach a fixed value as D_{wk} is reduced. Rather, the mean drag continues to drop, while the magnitude of the oscillations increase, at the lower D_{wk} values. This is probably a hysteresis effect, aggravated by the extremely fine grid spacing near the surface, that would vanish at a large number of iterations. The pressure coefficient data is not strongly affected by the oscillations introduced by low values of D_{wk}. Figure 13 provides pressure data at four locations of an oscillation when D_{wk} equals 20. There is very little effect on shock location or the flow upstream of the shock. What effects there

are appear to be confined to the foot of the shocks and the nearby separated regions.

New Results

As a final test of the modified separated-flow/wake eddy-viscosity model, a new solution, starting with free-stream conditions everywhere, was initiated for the Mach = 0.807, α = 0.36, Reynolds number = 6.2 x 10^6 case with D_{wk} = 50. This value was chosen for D_{wk} because it appears to be large enough to provide a non-oscillatory solution, yet small enough to be in the constant range for C_L. The solution was essentially converged after 20,000 iterations. Another 20,000 iterations were computed just to make sure the convergence was really stable (Figure 14). Figure 15 shows pressure coefficient results compared to experimental pressure coefficients. Converged solutions were also obtained for Reynolds numbers of 12.0 x 10^6 and 2.0 x 10^6 to evaluate Reynolds number effects on the value for D_{wk}. The value for D_{wk} should be the smallest value that provides a non-oscillatory (or acceptably small oscillatory) solution.

III. CONCLUSIONS

Governing equations for the flow of an ideal gas, and a review of the process involved in a numerical solution of the resulting Navier-Stokes equations has been provided. This includes a discussion of finite difference algorithms, boundary conditions, computational mesh (grid) generation and the development of an algebraic turbulence model.

Unfortunately, numerical solutions of the governing equations for flow fields with turbulent boundary layers and strong shock-induced separation that match experimental data has been beyond the state of the art. The limiting problem was associated with the closure model for the Reynolds averaged Navier-Stokes equations. This report describes a modification to the Baldwin-Lomax algebraic eddy-viscosity turbulence model that appears to do a very good job of predicting shock location on both the upper and lower surfaces. The computed shock is not quite as sharp as the experimental data, but this could be due to a lack of grid resolution at the shock location. The shape of the pressure distribution in the separated region is well modeled; however, the level of the pressures are somewhat high (low negative pressure coefficients). There also appears to be a small discrepancy in the pressures on the upper surface ahead of the shock. The boundary conditions imposed by the wind tunnel walls could have a significant effect. Also, grid resolution can be contributing to the lack of agreement. The grid used for this study clusters points near the surface, which would be more appropriate for an attached, viscous flow. When the flow separates the high gradient velocity region lifts off the surface (Figure 16) and is in an area with relatively sparse grid points.

Additional research is needed to verify the procedure for different airfoils and test conditions. Additional work is also needed to investigate values for two new variables in the turbulence model, D_{wk} and Y_o. At this time the recommended approach for defining D_{wk} is to pick the smallest value that will provide a solution with acceptably small oscillations in the shock location. The choice of Y_o as the height of the

reverse flow region is also rather arbitrary. Any length scale that is proportional to the magnitude of separation could be used. Perhaps with some additional study a combination of Y_o and D_{wk} that would work for a wide variety of airfoils could be determined. The applicability of this procedure to three-dimensional flow also needs to be investigated.

REFERENCES

1. White, F. M., Viscous Fluid Flow, McGraw-Hill, 1974.

2. Hankey, W. L., "Introduction to Computational Aerodynamics," AFWAL-TR-82-3031, Apr 1983.

3. Malvern, L. E., Introduction to the Mechanics of a Continuous Medium, Prentice-Hall, 1969.

4. Jameson, A., Schmidt, E. and Turkel, E., "Numerical Solution of Euler Equations by Finite Volume Methods Using Runge-Kutta Time Stepping Scheme," AIAA paper 81-1259, 1981.

5. Anderson, D. A., Tannehill, J. C. and Pletcher, R. H., Computational Fluid Mechanics and Heat Transfer, Mcgraw-Hill, 1984.

6. Ketter, R. L. and Sherwood, P. P., Modern Methods of Engineering Computation, McGraw-Hill, 1969.

7. Roache, P. J., Computational Fluid Dynamics, Hermosa Publishers, Albuquerque, N. M., 1972.

8. MacCormack, R. W., "The Effects of Viscosity in Hypersonic Impact Cratering," AIAA paper 69-354, 1969.

9. Courant, R., Friedrichs, K. O., and Lewy, H., "Uber die Partiellen Differenzengleichungen der Mathematischen Physik," Mathematische Annalen, Vol. 100, pp 32-74, 1928 (Translated in: IBM Journal of Research and Development, Vol. 11, pp 215-234 Mar 1967).

10. Schlichting, H., Boundary Layer Theory, McGraw-Hill, 1960.

11. Baldwin, B. S. and Lomax, H., "Thin Layer Approximation and Algebraic Model for Separated Turbulent Flows," AIAA paper 78-257, Jan 1978.

12. Cebeci, T., Smith, A. M. O. and Mosinski, G., "Calculation of Compressible Adiabatic Turbulent Boundary Layers," AIAA Journal, Vol. 8, No. 11, Nov 1970, pp 1974-1982.

13. Jobe, C. E. and Hankey, W. L., "Turbulent Boundary Layer Calculations in Adverse Pressure Gradient Flows," AIAA Journal Vol. 18, No. 11, Nov 1980, pp 1394-1397.

14. Visbal, M. and Knight, D., "Evaluation of the Baldwin-Lomax Turbulence Model for Two-Dimensional Shock Wave Boundary Layer Interactions," AIAA paper 83-1697, Jul 1983.

15. Shang, J. S., Hankey, W. L. and Dwoyer, D. L., "Numerical Analysis of Eddy Viscosity Models in Supersonic Turbulent Boundary Layers," ARL 74-0044, Dec 1973.

16. Shang, J. S., "An Assessment of Numerical Solutions of the Compressible Navier-Stokes Equations," Journal of Aircraft, Vol. 22, No. 5, May 1985, pp 353-370.

17. Lakshminarayana, B., "Turbulence Modeling for Complex Shear Flows," AIAA Journal, Vol. 24, No. 12, Dec 1986, pp 1900-1917.

18. Marvin, J. G., "Turbulence Modeling for Computational Aerodynamics," AIAA Journal, Vol. 21, No. 7, Jul 1973, pp 941-955.

19. Williams, W. E., Partial Differential Equations, Oxford Applied Mathematics and Computing Science Series, Oxford University Press, 1980.

20. Temam, R., Navier-Stokes Equations and Nonlinear Function Analysis, Society for Industrial and Applied Mathematics, Philadelphia, 1983.

21. Steger, J. L., Pulliam, T. H. and Chima, R. V., "An Implicit Finite Difference Code for Inviscid and Viscous Cascade Flow," AIAA paper 80-1427, Jul 1980.

22. Thomas, J. L. and Salas, M. D., "Far-Field Boundary Conditions for Transonic Lifting Solutions to the Euler Equations," AIAA paper 85-0020, Jan 1985.

23. Rudy, D. H. and Strikwerda, J. C., "Boundary Conditions for Subsonic Compressible Navier-Stokes Calculations," Computer and Fluids, Vol. 9, 1981, pp 327-338.

24. Shang, J. S., "Oscillatory Compressible Flow Around a Cylinder," AIAA paper 82-0098, Jan 1982.

25. Jameson, A. and Baker, T. J., "Solution of the Euler Equations for Complex Configurations," AIAA paper 83-1929, 1983.

26. Visbal, M. R., and Shang, J. S., "A Comparison Study Between an Implicit and Explicit Algorithm for Transonic Airfoils," AIAA paper 85-0480, Jan 1985.

27. Thompson, J. F., Warsi, Z. U. A. and Mastin, C. W., Numerical Grid Generation Foundations and Applications, North-Holland, 1985.

28. Steger, J. L. and Chaussee, D. S., "Generation of Body Fitted Coordinates Using Hyperbolic Partial Differential Equations," SIAM J. Sci. Stat. Comput., Vol 1, No. 4, Dec 1980, pp 431-437.

29. Edwards, T. A., "Noniterative Three-Dimensional Grid Generation Using Parabolic Partial Differential Equations," AIAA paper 85-0485, Jan 1985.

30. Vinokur, M., "On One-Dimensional Stretching Functions for Finite Difference Calculations," NASA CR 3313, Oct 1980.

31. Beam, R. W. and Warming, R. F., "An Implicit Finite-Difference Algorithm for Hyperbolic Systems in Conservation Law Form," J. Comp. Phys., Vol. 22, 1976, pp 87-110.

32. Davis, S. S. and Malcolm, G. N., "Experimental Unsteady Aerodynamics of Conventional and Supercritical Airfoils," NASA TM 81221, Aug 1980.

33. Pulliam, T. H., "Recent Improvements in Efficiency, Accuracy, and Convergence for Implicit Approximate Factorization Algorithms," AIAA paper 85-0360, 1985.

34. Metha, U. and Lomax, H., "Reynolds Averaged Navier-Stokes Computations of Transonic Flows-The State of the Art," Transonic Aerodynamics, AIAA, New York, 1982.

35. Johnson, D. A., "Predictions of Transonic Separated Flow with an Eddy-Viscosity/Reynolds-Shear-Stress Closure Model," AIAA paper 85-1683, Jul 1985.

Table 1

Riemann invariant Far Field Boundary Conditions*

	In Flow Boundary	Out Flow Boundary
Supersonic Flow at Boundary	All variables set to free stream values.	All variables extrapolated from the interior.
Subsonic Flow at Boundary	$V_{tangential}$ and entropy set to freestream values.	$V_{tangential}$ and entropy extrapolated from interior.
	V_{normal} and speed of sound computed from fixed and extrapolated Riemann invariants.	
	Density and pressure calculated from entropy and speed of sound.	

* Courtesy of Pradeep Raj, Lockheed-California Company

Table 2

Values for Parameters in Grid Code

Variable	Computer Symbol	Value	Comment
i_{max}	JMAX	340	Number of points around the body and wake cutline.
j_{max}	KMAX	85	Number of grid levels away from the body to the far field.
$\Delta\eta$	SETA	0.0001	Initial step size away from the body.
η_{max}	SETMX	15	Far field location in chord lengths.
	ESCAL	0.00127	Factor controlling the rate at which the grid attempts to provide equal cell areas.
σ_1	SMUIM	0.005	Explicit smoothing parameter.
σ_2	SMU	0.005	Implicit smoothing parameter.
α	ALPHA	1 to 2.5	Factor that changes the finite difference approximation. Varies as a function of grid level.

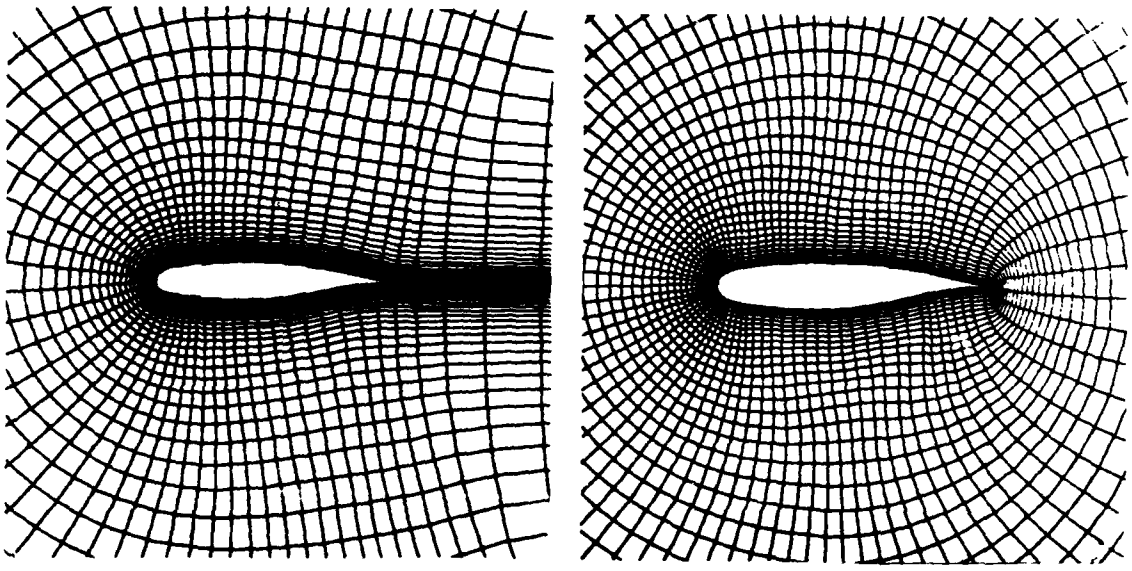

C-Type Grid O-Type Grid

Figure 1. O-Type and C-Type Grids on NLR-7301 Airfoil

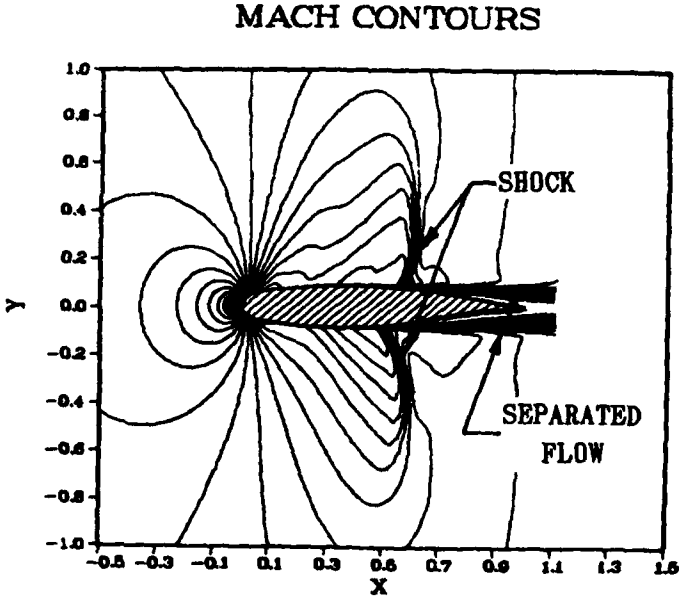

Figure 2. NLR-7301 Airfoil with Strong Shocks and Separated Flow, Mach=0.807, α=0.37, R_n=12X10^6

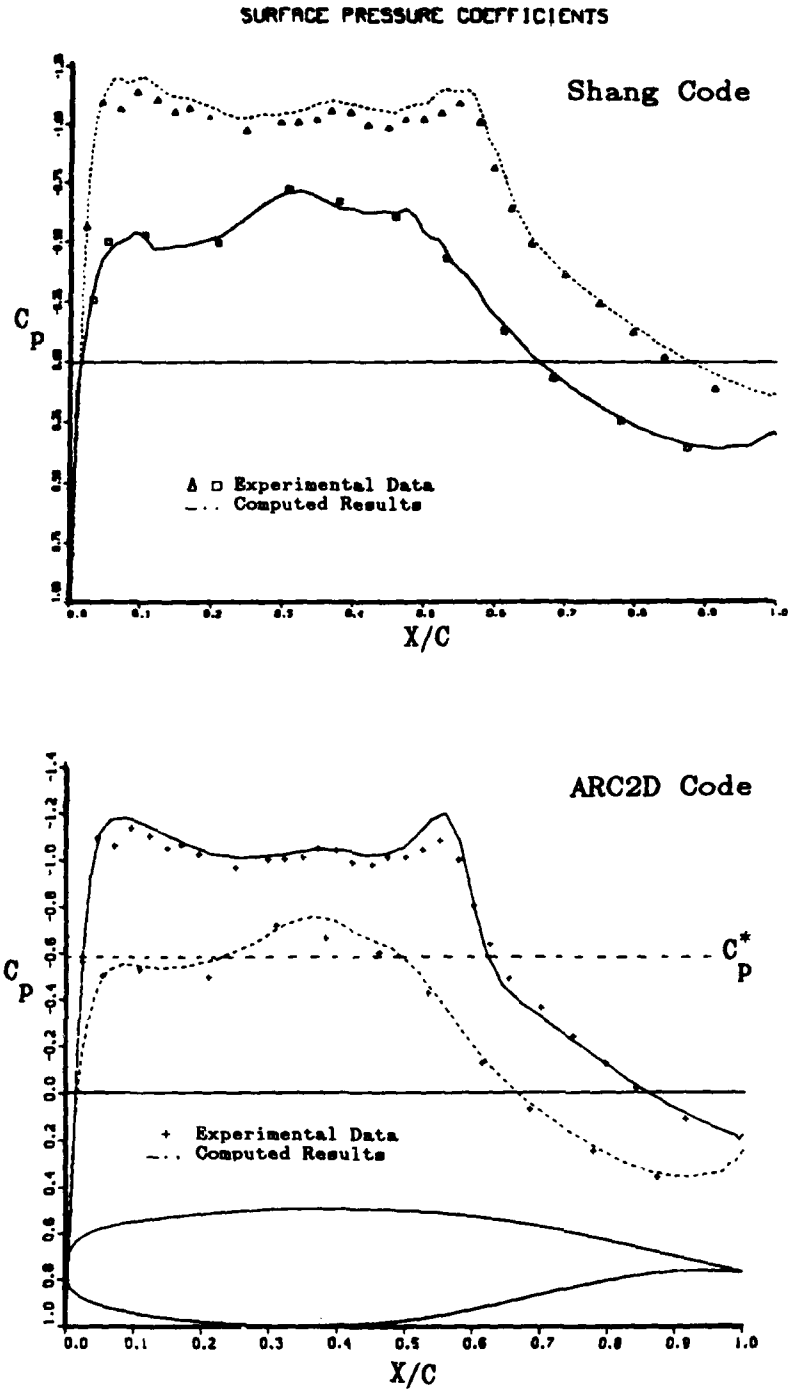

Figure 3 Comparison of Shang and ARC2D Codes, Mach=0.752, α=0.37, R_n=6.2X10^6

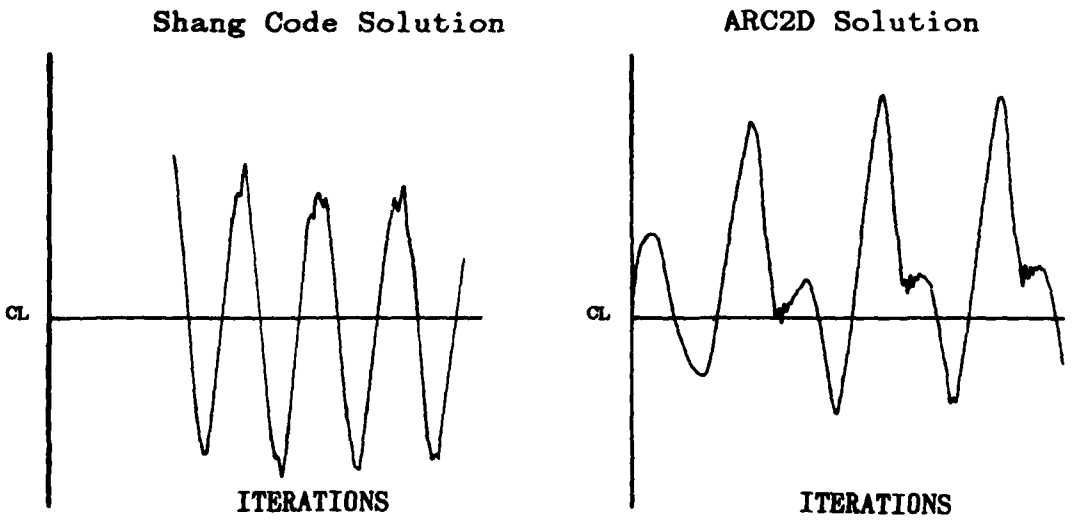

Figure 4 Oscillating Solutions at Mach = 0.807

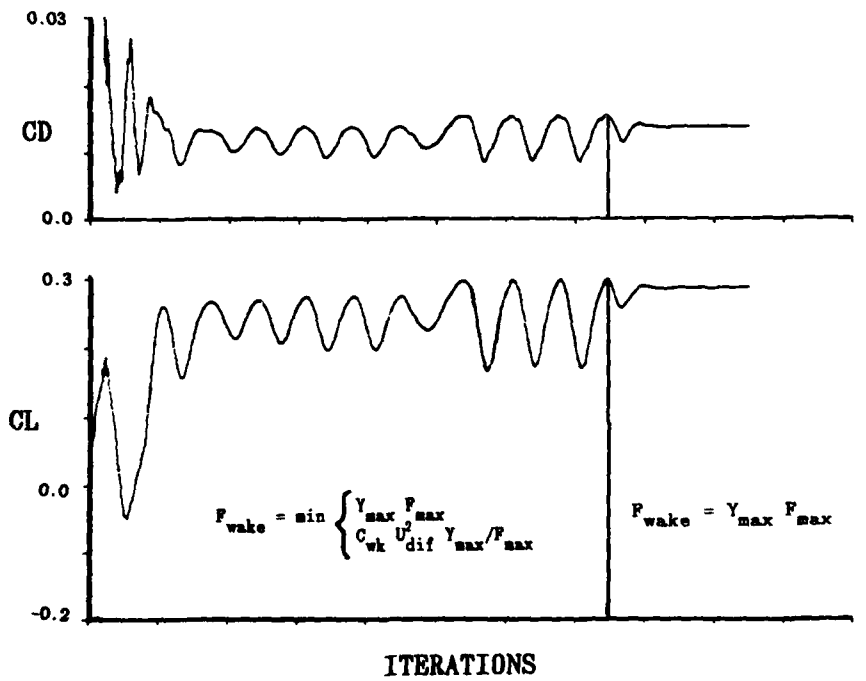

Figure 5 Oscillations at Mach=0.75

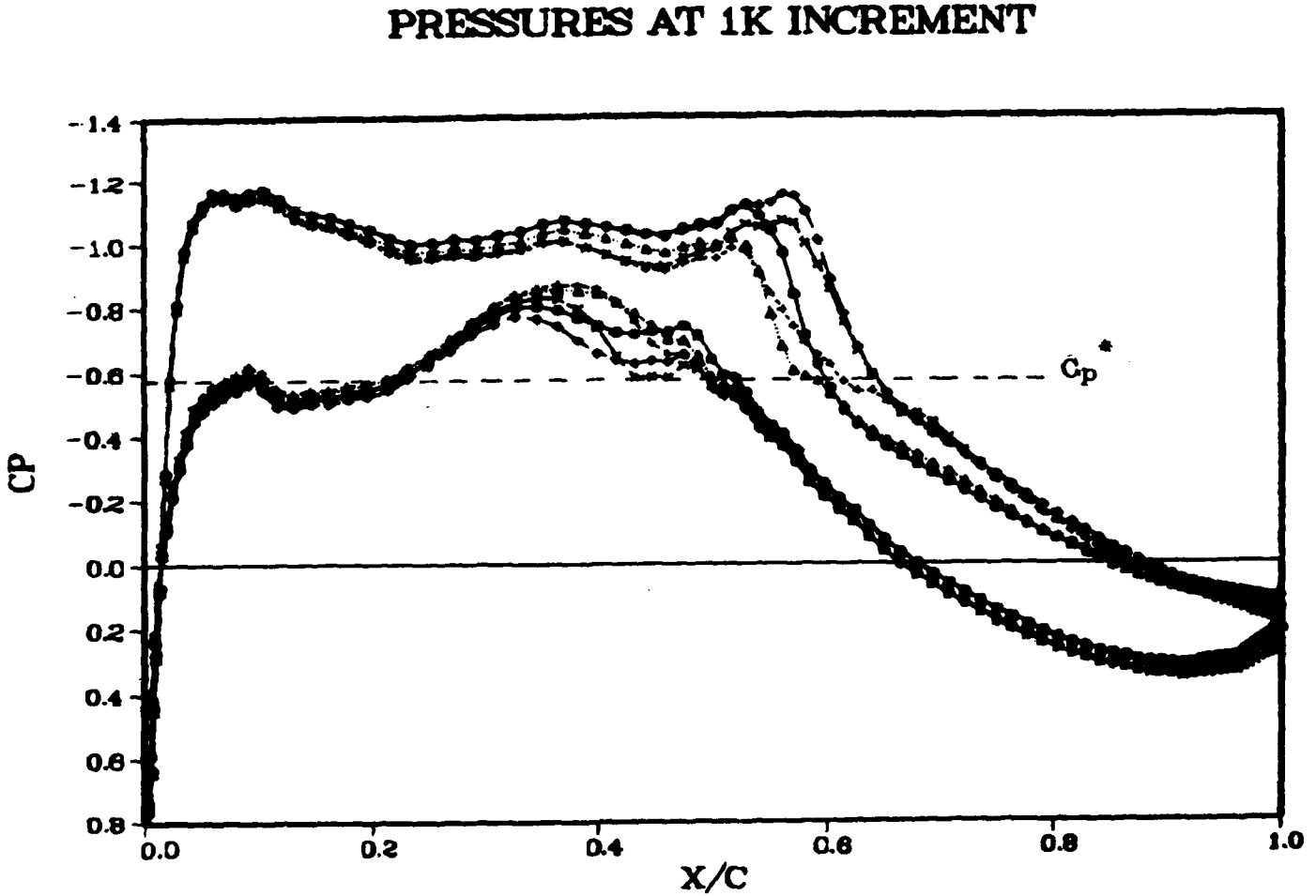

Figure 6 Mach=0.75 Range of Pressure Distributions

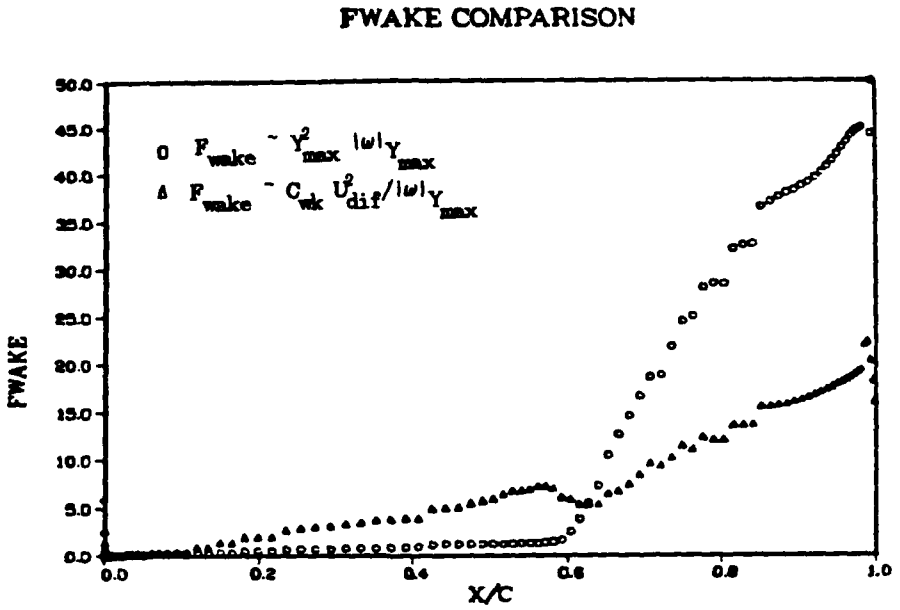

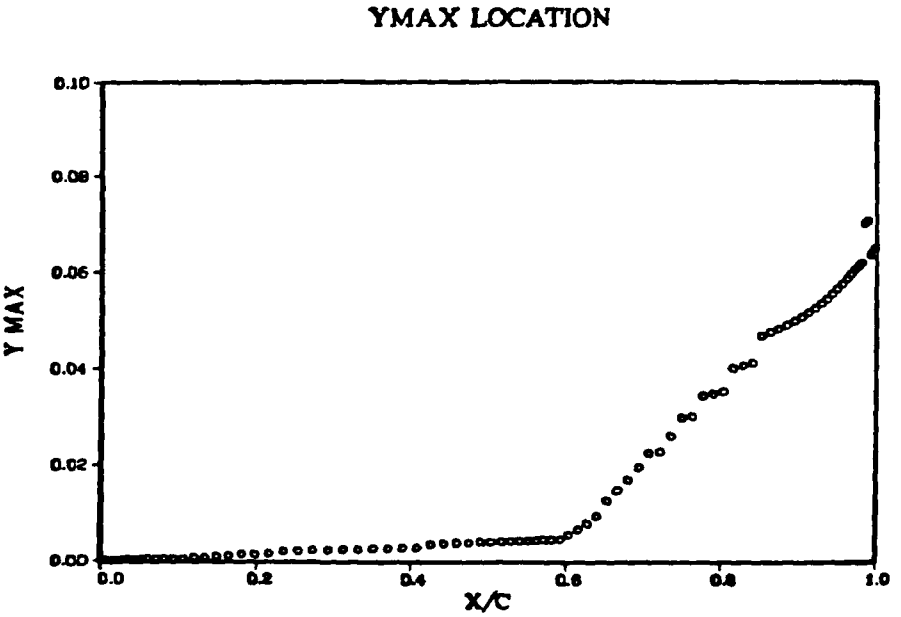

Figure 7 F_{wake} and Y_{max} for Mach=0.807, α=0.37, R_n=6.2X10^6

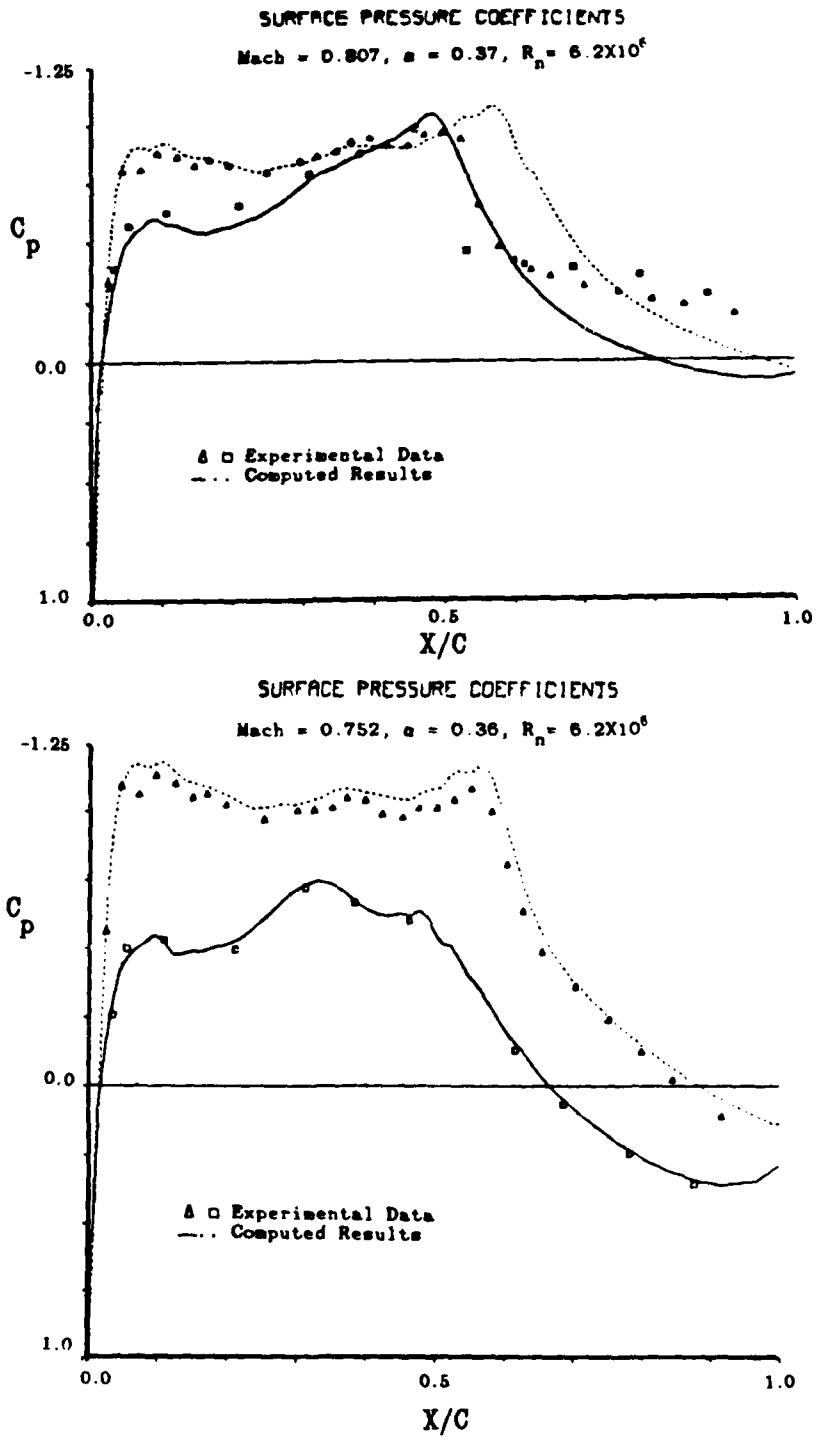

Figure 8 Mach=0.807 and 0.752 Solutions with $F_{wake}=Y^2_{max}|\omega|_{max}$

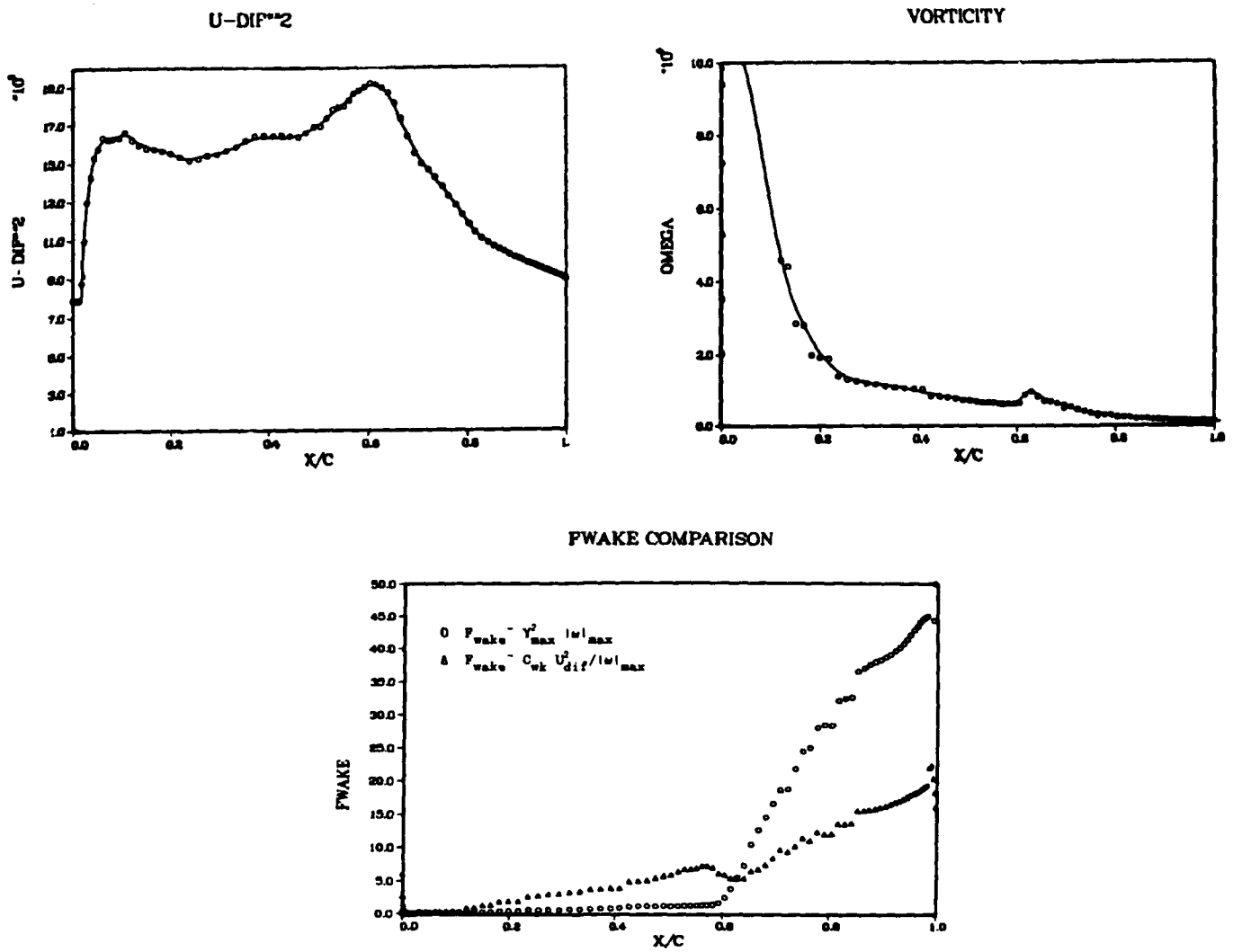

Figure 9 U^2_{dif}, $|\omega|_{max}$ and F_{wake} for Mach=0.807 Oscillatory Flow

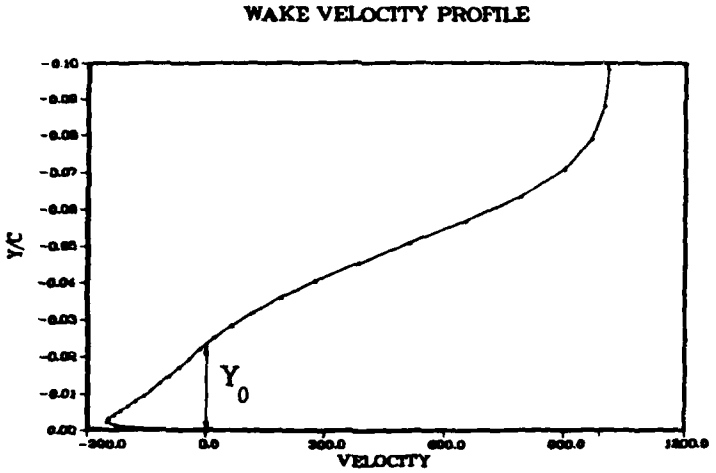

Lower Surface @ 80% X/C

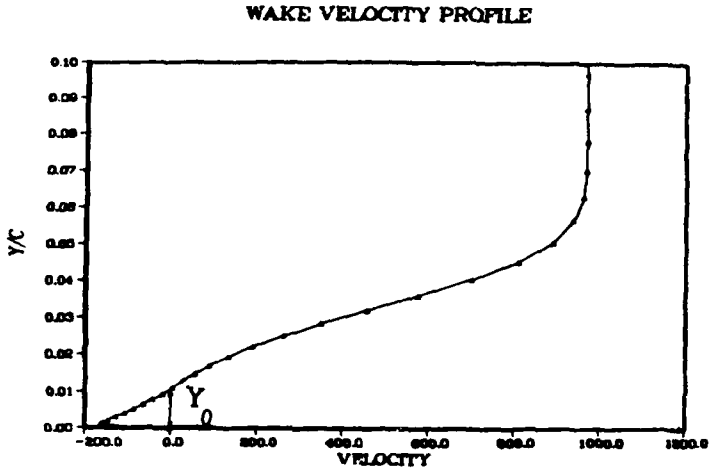

Upper Surface @ 80% X/C

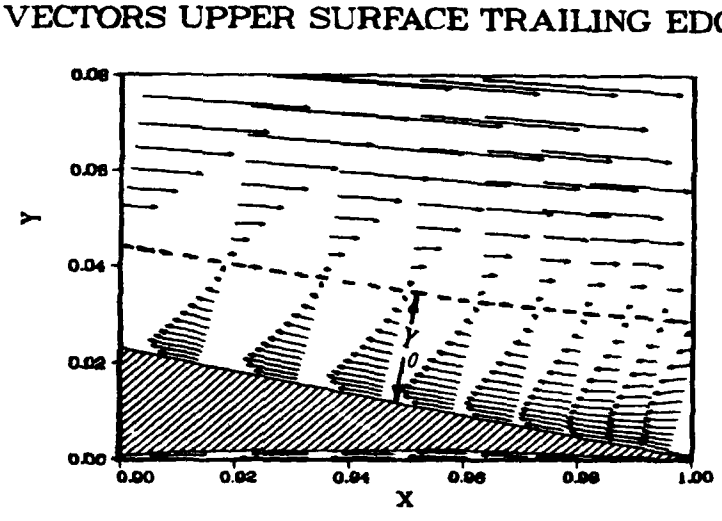

Figure 10 Reversed Flow in Separated Region, Mach=0.807, α=0.37

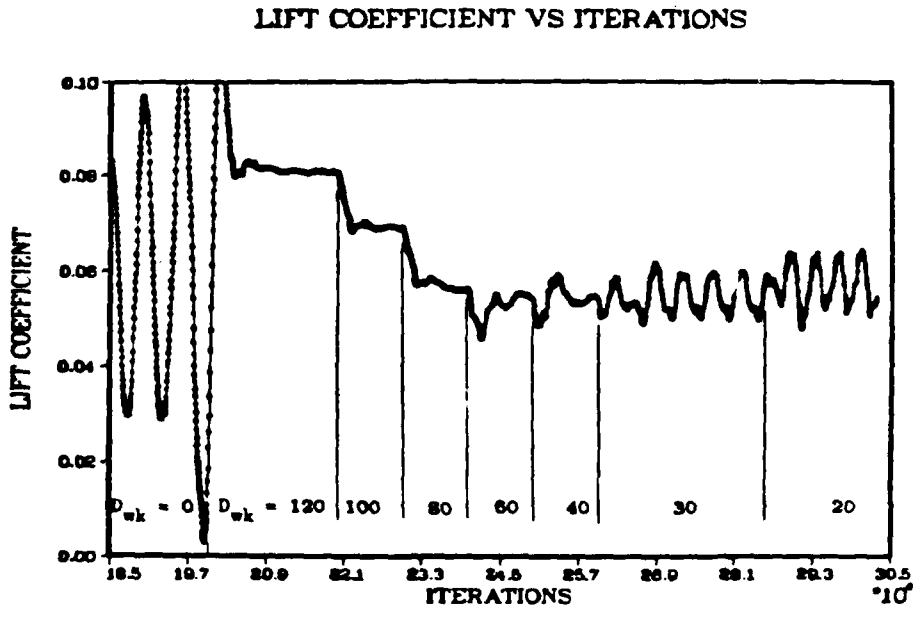

Figure 11 Effects of D_{wk} on Lift, Mach=0.807, α=0.37, R_n=6.2X10^6

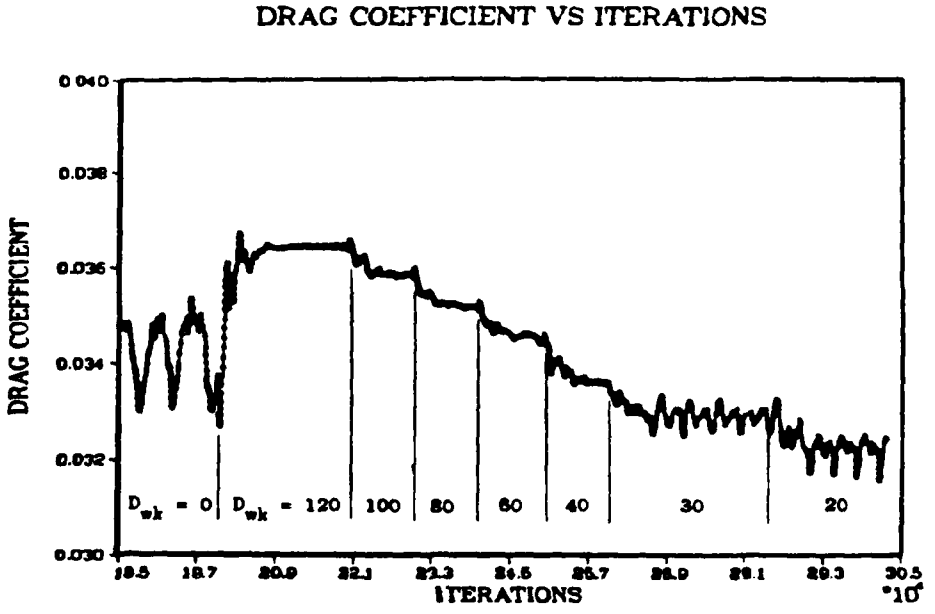

Figure 12 Effects of D_{wk} on Drag, Mach=0.807, α=0.37, R_n=6.2X10^6

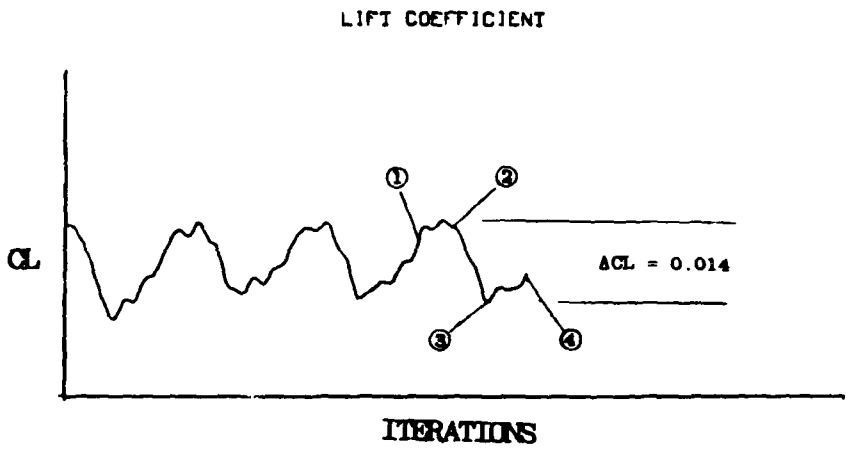

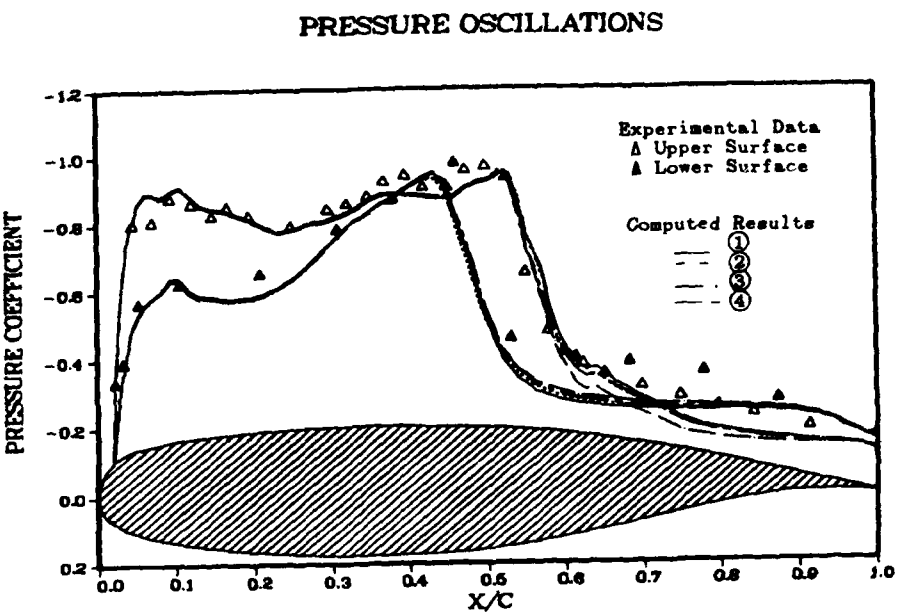

Figure 13 Effects of Oscillations in C_L on Pressures,

Mach=0.807, α=0.37, R_n=6.2X10^6

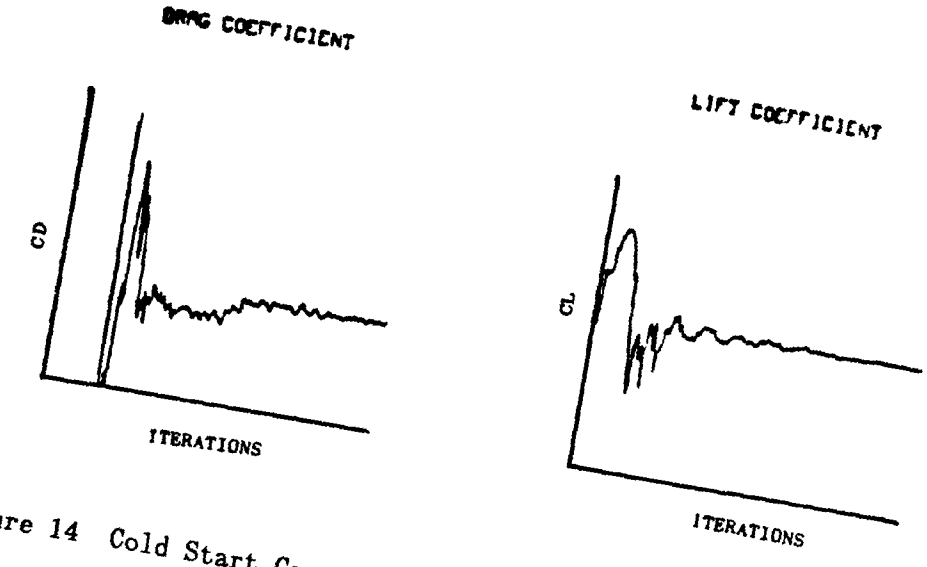

Figure 14 Cold Start Convergence, Mach=0.807, α=0.37, R_n=6.2X10^6, D_{wk}=50

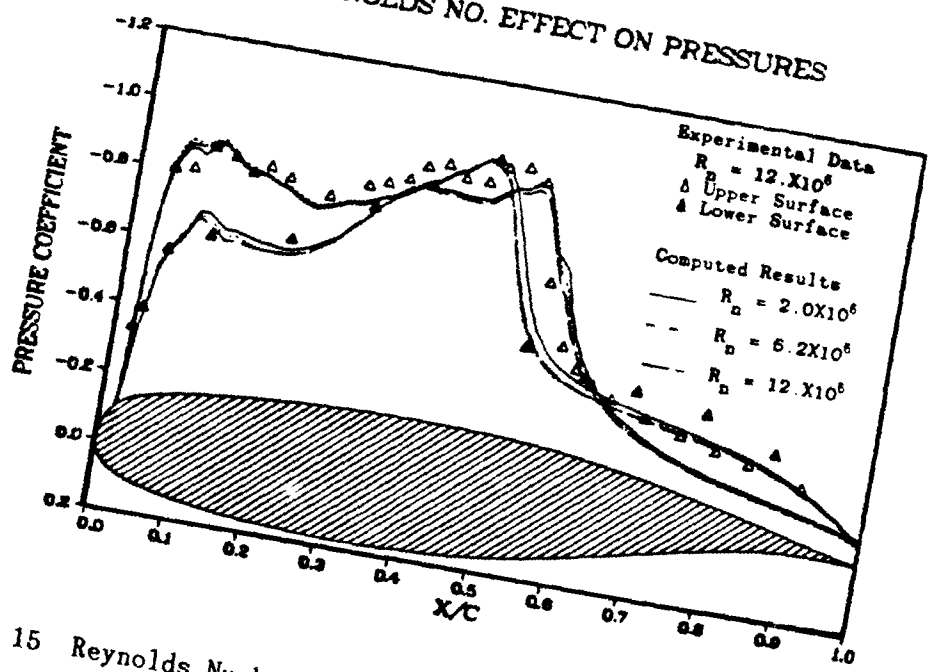

Figure 15 Reynolds Number Effects, Mach=0.807, α=0.37, D_{wk}=50

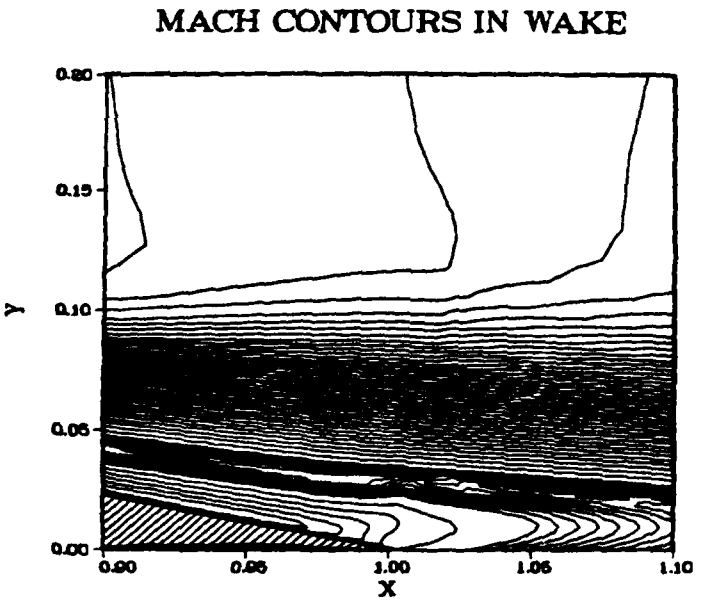

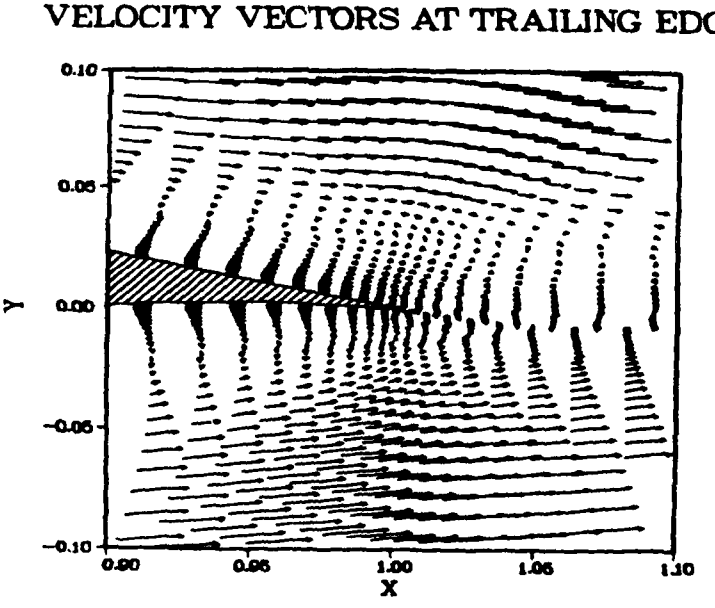

Figure 16 Trailing Edge Flow Conditions, Mach=0.807, α=0.36, R_n=12.X10^6, D_{wk}=50

LIST OF SYMBOLS

A	Surface area of an arbitrary volume
A^+	Sublayer constant for turbulence model
B	Matrix defined in grid development
C	Matrix defined in grid development
C_{cp}	Constant in turbulence modeling
C_{kleb}	Klebanoff constant in turbulence modeling
C_L	Lift coefficient
C_p	Constant pressure specific heat
C_v	Constant volume specific heat
C_{wk}	Constant in turbulence modeling
c	Speed of sound
D	van Driest damping function
D_{wk}	Variable in turbulence modeling
F	Flux vector in governing equations
F_{kleb}	Klebanoff intermittency function
F_{max}	Function in turbulence modeling
F_{wake}	Function in turbulence modeling
$\hat{f}$	Right hand side vector in grid development
f	Arbitrary variable
G	Flux vector in governing equations
i	Index representing current x or ξ location
j	Index representing current y or η location
n	Index representing current time step
K	Clauser constant in turbulence modeling
$\hat{k}$	Thermal conductivity coefficient
k	von Karman constant
k_t	Eddy conductivity coefficient

$\vec{\vec{P}}$	Dyadic representing stresses
p	Hydrostatic pressure
Pr_t	Turbulent Prandtl number
$\vec{\vec{Q}}$	Arbitrary tensor
$\vec{q}$	Heat flux vector
$\vec{R}$	Vector in grid development
R	Gas constant
R_n	Reynolds number
T	Temperature
t	Time dimension
$\vec{U}$	Velocity vector
U	Vector of flow variables in governing equations
u	Velocity in the x direction
V	Arbitrary control volume
v	Velocity in the y direction
x	Cartesian coordinate
y	Cartesian coordinate

Greek:

$\hat{\alpha}$	Constant in MacCormack pressure damping
α	Angle of attack
δ	Finite difference operator
ϵ	Eddy-viscosity coefficient
η	Transformed coordinate for y
γ	Ratio of specific heats
ℓ	Length scale for turbulence modeling
λ	Coefficient of bulk viscosity
μ	Coefficient of shear viscosity
ρ	Density (mass per unit volume)
σ	Smoothing parameter in grid development
τ	Stress on a fluid element

ω	Vorticity
ξ	Transformed coordinate for x
Δ	Incremental values
$\hat{\Delta}$	Dissipation operator in grid development
∇	Divergence operator
$\hat{\nabla}$	Dissipation operator in grid development